Chem Soc Rev

REVIEW ARTICLE

View Article Online
View Journal

Cite this: DOI: 10.1039/c8cs00470f

Azobenzene-based solar thermal fuels: design, properties, and applications

Liqi Dong, [a] Yiyu Feng, [a] Ling Wang [a] and Wei Feng *[abcd]

Development of renewable energy technologies has been a significant area of research amongst scientists with the aim of attaining a sustainable world society. Solar thermal fuels that can capture, convert, store, and release solar energy in the form of heat through reversible photoisomerization of molecular photoswitches such as azobenzene derivatives are currently in the limelight of research. Herein, we provide a state-of-the-art account on the recent advancements in solar thermal fuels based on azobenzene photoswitches. We begin with an overview on the importance of azobenzene-based solar thermal fuels and their fundamentals. Then, we highlight the recent advances in diverse azobenzene materials for solar thermal fuels such as pure azobenzene derivatives, nanocarbon-templated azobenzene, and polymer-templated azobenzene. The basic design concepts of these advanced solar energy storage materials are discussed, and their promising applications are highlighted. We then introduce the recent endeavors in the molecular design of azobenzene derivatives toward efficient solar thermal fuels, and conclude with new perspectives on the future scope, opportunities and challenges. It is expected that continuous pioneering research involving scientists and engineers from diverse technological backgrounds could trigger the rapid advancement of this important interdisciplinary field, which embraces chemistry, physics, engineering, nanoscience, nanotechnology, materials science, polymer science, *etc.*

Received 14th June 2018

DOI: 10.1039/c8cs00470f

rsc.li/chem-soc-rev

[a] *School of Materials Science and Engineering, Tianjin University, Tianjin 300072, P. R. China. E-mail: weifeng@tju.edu.cn; Fax: +86 22 27404724; Tel: +86 22 87402059*
[b] *Collaborative Innovation Center of Chemical Science and Engineering, Tianjin 300072, P. R. China*
[c] *Key Laboratory of Advanced Ceramics and Machining Technology, Ministry of Education, Tianjin 300072, P. R. China*
[d] *Tianjin Key Laboratory of Composite and Functional Materials, Tianjin 300072, P. R. China*

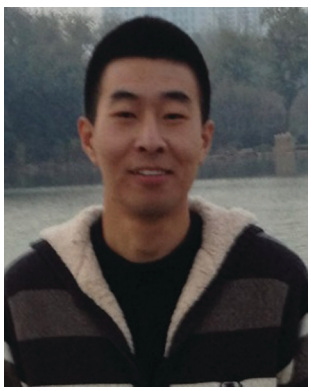

Liqi Dong

Liqi Dong received his BS degree in Chemistry from Qingdao University of Science & Technology (China) in 2013 and completed his MS degree under the supervision of Prof. Xuemin Duan and Prof. Jingkun Xu at Jiangxi Science & Technology Normal University (China) in 2016. He is now pursuing his PhD degree under the tutelage of Prof. Wei Feng at the School of Materials Science and Engineering, Tianjin University. Currently, his research is focused on solar energy harvesting and conversion and storage solution based on photo-responsive molecules.

Yiyu Feng

Yiyu Feng is a research professor at the School of Materials Science and Engineering, Tianjin University. He obtained his PhD from Tianjin University in 2009 and held an academic position at Tianjin University in 2009. He has authored and co-authored over 80 academic articles and reviews. Currently, his research is focused on solar-thermal conversion and thermal interfacial materials and composites, as well as their application in heat-control systems.

1. Introduction

Fossil fuel depletion, global warming, and the hidden risks of international conflict are weaving an uncomfortable stranglehold on the world's energy outlook. Coping with these crises requires the development of renewable and sustainable energy technologies and strategies to reduce the dependence on traditional fossil fuels that are currently the main driving force of global economy.[1] Often-cited alternatives include clean coal, nuclear energy, and a host of renewable energy sources such as biomass/biofuels, hydroelectric power, geothermal energy, ocean water, tides, waves, wind, and solar energy.[2–4] Among them, solar energy is the most abundant and inexhaustible natural resource in our solar system: the sun delivers in 1 h what humankind needs in a year.[2,5] Vast amounts of energy enter our atmosphere every day; however, efficient conversion of diffuse sunlight into useful forms of energy is quite a challenge. Toward this end, extensive efforts have been devoted to developing innovative technologies, especially to capture, convert, and store solar energy.[6] Nowadays, a variety of technologies have been proposed to harvest the abundant solar energy and reach a sustainable world society (Fig. 1). For example, photovoltaics[7–12] could directly convert sunlight into electrical power without any heat engine. Photovoltaic solar cells have seen a dramatic development in the past few years, mainly because of their simple design and structure, flexible installation, avoidance of long-distance transmission, and cost reduction.[13,14] Solar thermal collectors[15–21] are able to absorb the incoming solar radiation, convert it into heat, and transfer this heat to a fluid (usually air, water or oil) flowing through the collector. There are basically two types of solar collectors: non-concentrating or stationary and concentrating. The temperature range varies with the types of collectors, such as flat-plate collectors, 30–90 °C; evacuated tube collectors, 50–200 °C; parabolic dish reflectors, 100–500 °C; heliostat field collectors, 150–2000 °C.[15] Depending on the temperature level, the heat

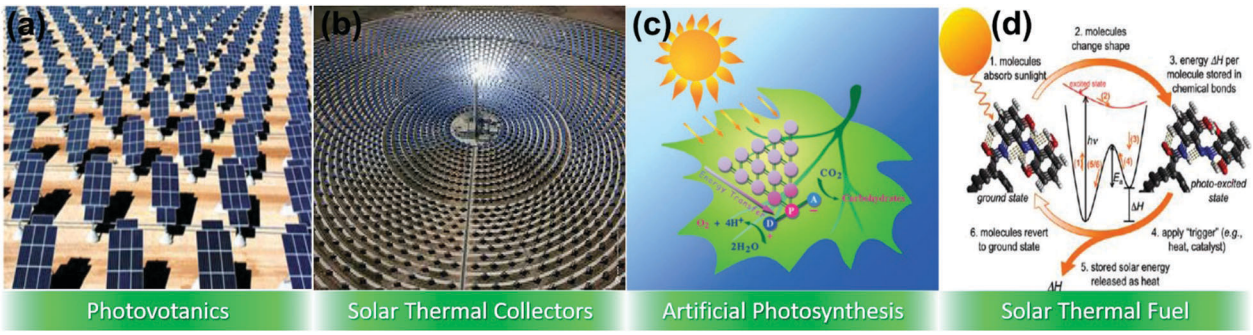

Fig. 1 Emerging technologies for capture, conversion, and storage of solar energy: (a) photovoltaics; reprinted with permission from ref. 6. Copyright 2011 Royal Society of Chemistry. (b) Solar thermal collectors; reprinted with permission from ref. 21. Copyright 2014 Elsevier Ltd. (c) Artificial photosynthesis; reprinted with permission from ref. 1. Copyright 2007 Wiley-VCH. (d) Solar thermal fuels. Reprinted with permission from ref. 133. Copyright 2011 American Chemical Society.

Ling Wang

Ling Wang is a professor at the School of Materials Science and Engineering in Tianjin University (China). He received his PhD degree from the University of Science and Technology Beijing (China) in 2013. From 2013 to 2018, he worked as a postdoctoral research fellow at the Liquid Crystal Institute of Kent State University (USA) and the Artie McFerrin Department of Chemical Engineering at Texas A&M University (USA), respectively. His research interests include design, synthesis, and properties of molecular switches, photoactive soft materials or polymers, functional nanoparticles, and 2D nanomaterials, as well as their emerging applications in diverse fields ranging from dynamic photonics to energy and safety issues.

Wei Feng

Wei Feng is a professor at the School of Materials Science and Engineering in Tianjin University. He obtained his PhD degree from the Xi'an Jiaotong University (China) in 2000. Then, he worked at Osaka University and Tsinghua University as a JSPS fellow and postdoctoral researcher, respectively. In 2004, he became a full professor in Tianjin University. He has obtained the support of National Science Fund for Distinguished Young Scholars in China. His research interests include photo-responsive organic molecules and their derivatives, thermal-conductive and high-strength carbon-based composites, and two-dimensional fluorinated carbon materials and polymers.

can be employed in industrial production to generate electricity or storable heat, to desalinate salt water, or to synthesize fuels from water and carbon dioxide for storage, transportation, or on-site application. Solar fuels[22–25] could collect solar energy and store it through the energetic chemical bonds, where the solar harvesting and energy storage processes are incorporated in a single entity. This approach has been investigated in several variations including CO reduction, CO_2 reduction, photoinduced water splitting (*i.e.*, artificial photosynthesis) *etc.* Interestingly, solar thermal fuels based on photoactive materials have recently attracted increasing attention, where the efficient absorption of solar irradiation leads to a photoisomerization reaction towards a high-energy species, thus enabling the storage of large amounts of heat.[6,26,27]

Solar thermal fuels (STFs) can store the energy from solar radiation through structural and bond rearrangements of the photoactive materials, and then the energy is released in the form of heat. Such a closed cycle enables reversible solar conversion and energy storage within a single material system. STFs have attractive advantages including no emission, easy transportation, rechargeability and renewability, and on-demand energy release in the form of heat. STFs have started to receive increasing attention since the 1970s, probably as a result of the 1973 oil crisis. Since then, diverse types of molecular photoswitches have been developed for STFs (Fig. 2). For example, anthracene, a rigid aromatic hydrocarbon, undergoes [4+4] cycloaddition to form a dimer when exposed to light at 400 nm, and then a stored heat energy of 65.2 kJ mol^{-1} can be released through appropriate thermal treatment or light irradiation at below 300 nm.[28–30] The storage enthalpy ($\Delta H_{storage}$, the maximum energy that can be stored per mole of photoactive molecules) could be increased to 83.6 kJ mol^{-1} by grafting electron-withdrawing groups (EWGs) and electron-donating groups (EDGs) onto the anthracene monomer. However, the quantum yield for the forward reaction is dependent on the relative concentration.[28,30–32] Recently, Castellano's research group demonstrated the triplet–triplet annihilation-based photon upconversion properties of an anthracene system through incorporating a sensitizer (such as Ru(II) and Pd(II) octaethylporphyrin) and/or an acceptor (such as 9,10-diphenylanthracene and its derivatives).[33–38] Such photon upconversion systems are expected to offer an alternative way toward STFs with high molecular storage capacity.[39] Stilbenes undergo a *trans*-to-*cis* photoisomerization under light irradiation at wavelengths ranging from 300 to 700 nm.[40–43] Although stilbene has a low molecular weight, it is restricted by low $\Delta H_{storage}$ ($\sim$5 kJ mol^{-1}).[40,42–44] Mancini and co-workers investigated a range of 9-styrylacridines and discovered that the $\Delta H_{storage}$ could be considerably increased by introducing functional groups. The highest value (104 kJ mol^{-1}) was obtained by replacing the phenyl group with a 1-naphthyl group.[42,43] (Fulvalene)tetracarbonyldiruthenium ($FvRu_2(CO)_4$) refers to a series of organometallic photochromic complexes, which were first reported by Vollhardt and co-workers in 1983.[45,46] In solution, $FvRu_2(CO)_4$ undergoes reversible photoisomerization upon irradiation with visible light (470 nm).[45–54] The $\Delta H_{storage}$ comprises the overall standard (83 $\pm$ 6 kJ mol^{-1}) and activation energies (125 $\pm$ 8 kJ mol^{-1}).[48] The $FvRu_2(CO)_4$ complex is less likely to be attractive for practical applications owing to its high cost and high molecular weight of $\sim$442 g mol^{-1}. Iron has been used to replace the expensive ruthenium because of its low cost and light weight; however, no isolatable photoisomer can be formed in the iron analogue.[51] Besides, an osmium analogue exhibiting photoisomerization was developed; however, the isomerization is irreversible.[54] To date, commercially available norbornadiene–quadricyclane (NBD–QC) has been the most investigated system for STF applications.[55–65] NBD undergoes a photoinduced [2+2] cycloaddition to convert into its valence isomer–quadricyclane. The strained quadricyclane molecule could store a significant amount of energy ($\Delta H_{storage}$ = 96 kJ mol^{-1}), and such stored energy can be released in the form of heat under the influence of an external stimulus or catalysts. It should be noted that NBD only absorbs ultraviolet (UV) light, and cannot be isomerized by visible light in any range of wavelengths. To increase the quantum yield, the absorption needs to be red-shifted. One of the promising strategies to red-shift the absorption of NBD is to introduce EWGs, or both EWG and EDG at one of the C=C double bonds. It was also found that the introduction of substituents at the C=C bond helps increase the isomerization quantum yield.[64,65] The dihydroazulene–vinylheptafulvene (DHA–VHF) photoreaction

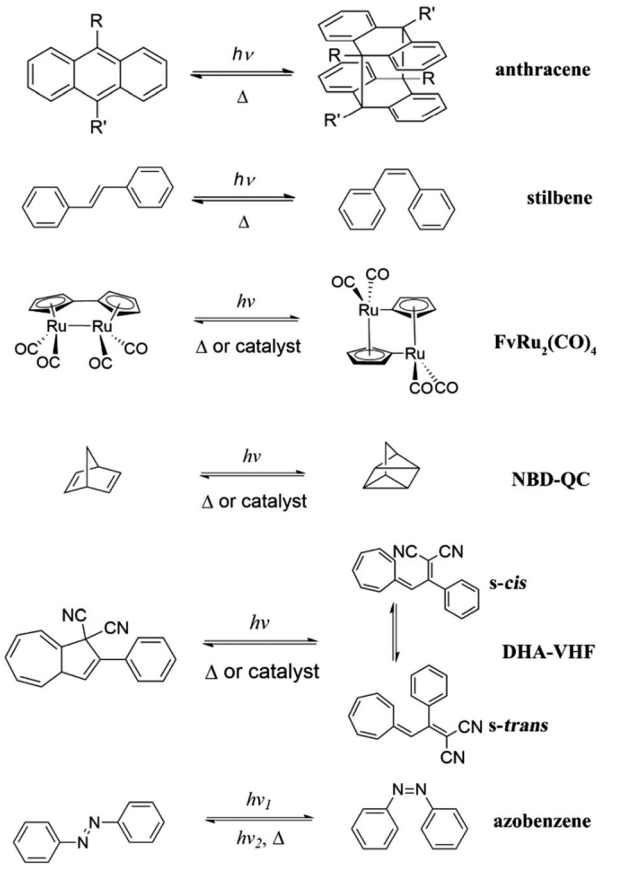

Fig. 2 Photoisomerization of different types of molecular photoswitches.

is a ring-opening reaction, which is characterized by a high quantum yield.[66–70] The large spectral difference between DHA and VHF (about 150 nm), the relatively high enthalpy of the photochemical reaction ($\Delta H_{storage}$ = 35.2 kJ mol^{-1}),[71] and the relatively long half-life (21 min to 26 h) make this system an interesting candidate for the development of STF application.[71–73] It should be noted that the back conversion of the DHA–VHF system can be stimulated by heating or catalysts (such as Cu(I)).[74,75] Moth-Poulsen *et al.* reported the solar energy storage of a DHA–VHF system under realistic outdoor conditions.[74] However, further reducing the spectroscopic overlap between the isomers should be taken into account in the future device and molecular designs.[66,72,76] Attempts have also been made to promote the performance of this STF system in terms of lifetimes and ED by introducing functional groups.[77] However, it remains a challenge to find the optimum molecule satisfying all the requirements.

In general, efficient STFs should meet the following set of criteria:[29,30] (i) solar spectrum match: the absorption of the low-energy isomer should overlap with the most intense region of the solar emission. (ii) Large storage energy capacity: the energy difference between low- and high-energy isomers relative to the molecular weight/volume should be as large as possible. (iii) High quantum yield: the photoinduced conversion towards the high-energy isomer should proceed with high efficiency. (iv) No photon competition: photon competition of two isomers should be avoided since both processes of photoisomerization and back-conversion in most of the photoactive molecules could be activated by light. (v) Long-term stability: the barrier for back-conversion on the ground state energy landscape should be sufficiently large to enable long-term storage and the photoactive materials should exhibit strong cyclability performance. (vi) Low price: the cost of the raw materials as well as synthesis and integration should be competitive.

Toward this end, azobenzene and its derivatives, the most widely investigated molecular photoswitches, emerging as a "star" material have recently attracted tremendous attention in the field of STFs. Pristine azobenzene can absorb UV light (365 nm) to convert solar energy into latent chemical energy and release heat through *cis*-to-*trans* isomerization by thermal relaxation or light irradiation at an appropriate wavelength. The $\Delta H_{storage}$ and quantum yield of pristine azobenzene were reported to be 49 kJ mol^{-1} and 0.49, respectively, and the half-life of *cis*-azobenzene was determined as 4.2 days.[78–81] It should be noted that azobenzene holds a large window of opportunities for rich chemical functionalization of the molecule. Azobenzene derivatives have facile synthesis, low cost, and extraordinary cycling stability through repeated photoisomerization and reverse isomerization between the *trans* and *cis* forms, all of which make them very attractive for STF applications.

The discovery of azobenzene can be dated back to the mid-1800s; however, for many years, they were only used as a class of synthetic coloring agents in the dye industry.[82] In the 1930s, apart from being used as simple dyes, colorants, or a pH indicator, azobenzene was discovered to possess photoisomerization capability.[83] From then on, design, synthesis and structure–property relationship of azobenzene photoswitches have been extensively explored by numerous industrial and academic research groups.[84–89] As a result, a variety of azobenzene derivatives with promising properties have been designed and synthesized. Based on its spectroscopic features, azobenzene is classified into three categories: azobenzene, aminoazobenzene, and pseudostilbene. The structure–property relationship of these azobenzene photoswitches with multifarious photoactive properties has also been well studied.[81] In the past decades, the photoisomerization characteristic of azobenzene and its use in the development of advanced functional materials have aroused considerable research enthusiasm, which promoted the applications of azobenzene and its derivatives as novel functional materials in diverse fields such as sensors,[90,91] actuators,[92–95] non-linear optic devices,[96–98] optical data storage,[99–101] and energy/biological materials.[86,102–104] Most recently, a variety of solar energy harvesting and storage solutions using azobenzene and its derivatives have been reported, which is expected to provide important impetus towards the rapid development of this highly interdisciplinary endeavor in photochemistry, nanoscience, nanotechnology, and energy-related intelligent advanced materials.[105,106]

This article provides a comprehensive review on the advancements in azobenzene-based STF (Azo-STF) materials concerning their fundamentals, diverse azobenzene types as STF materials, recent endeavors in the molecular design of azobenzene toward efficient STFs, and their promising applications. Although the study of solar thermal energy storage materials has already been reviewed in the past years,[6,27,79] to the best of our knowledge, a systematic review on the design, properties, and applications of Azo-STFs remains scarce. Herein, we focus on azobenzene derivatives, nanocarbon-templated azobenzene, and polymer-templated azobenzene, representing material platforms that combine solar energy harvesting and storage *via* the photoisomerization accorded by the azobenzene units. This review is structured as follows: first, we present an overview on the importance of Azo-STFs and their fundamentals in Section 2. In Section 3, we review the recent progress in Azo-STFs, with the aim of launching further research in this highly fascinating area. Section 4 is devoted to the recent endeavors in the molecular design of azobenzene derivatives toward efficient STFs. Finally, in Section 5, the basic design concepts of such advanced energy storage materials are discussed, their promising applications are highlighted, and new perspectives on the future scope, opportunities and challenges are addressed.

2. Fundamentals of azobenzene-based solar thermal fuels

2.1 Solar thermal conversion and energy storage using azobenzene photoswitches

STFs store solar energy through a photochemical conversion process known as photochromism. The idea of a STF was first proposed in 1909 by Weigert after observing the fuel capability of anthracene photodimerization.[28] This process, by definition,

is a reversible chemical conversion between two states, *e.g.*, A and B, induced in either one or both directions through the absorption of electromagnetic radiation. The two states possess different absorption or emission spectra owing to their different physical and chemical properties. State "A" represents the thermodynamically stable form, while state "B" is the metastable form transformed from state "A" through light irradiation. This structural change is reversible and the reverse process can occur through thermal relaxation or light irradiation at an appropriate wavelength. Ideally, for practical applications, the photochromic cycle could be repeated indefinitely although side reactions can occur that lead to subsequent degradation of the process.[106]

For a unimolecular system, photochromism can occur through several possible chemical processes and undergo transformation. Some of these chemical processes are bond cleavage, oxidation–reduction, and isomerization. Of these three, isomerization, or more specifically, photoisomerization, is the most favorable photochromism for STFs. Photoisomerization is divided largely into two types: *trans*-to-*cis* isomerization and valence isomerization. In the case of *trans*-to-*cis* isomerization, a noticeable structural change is observed, whereas in valence isomerization, no significant steric position difference is seen; rather, the electronic structures are rearranged.

For azobenzene, the isomerization process is *trans–cis* type, which shows a substantial quantum yield and characteristic differences between the *trans* and *cis* states. Therefore, azobenzene is one of the most excellent candidates for use as STFs. The photoisomerization of azobenzene is one of the special processes that dissipate the excessive energy of the species by controlling the molecular configurations. This change is often accompanied by other actions including radiationless/radiative transitions, vibration relaxation, and energy transfer quenching.[107] Until now, four mechanisms including inversion, rotation, concerted inversion, and inversion-assisted rotation have been proposed as possible pathways for azobenzene photoisomerization.[108–116] To understand these theories, we refer the interested readers to some previously published reviews.[6,81,107,110]

Here, we elucidate the principle of closed-system energy storage of STFs based on azobenzene photoswitches, as can be seen in Fig. 3. First, the azobenzene molecules exist in the *trans* conformation at room temperature, which corresponds to the ground state, also called the low-energy state. The ground state azobenzene molecule absorbs photon energy and transforms into an excited state, *i.e.*, the intermediate state. In the photoexcited state, azobenzene is very unstable and undergoes a conformational change within a few picoseconds.[114,117–119] Most of the photoexcited azobenzenes convert into the *cis*-isomer (productive relaxation) while a small number of molecules may revert to the original stable *trans*-isomer (unproductive relaxation).[118,120,121] In the new state, referred to as the metastable state, also called the high-energy state, energy is stored in the chemical bonds. To access this stored energy in azobenzene molecules, an external trigger such as heat or visible light is usually applied to overcome the energy barrier (ΔE_a). The stored solar energy is then released in the form of heat and the molecule reverts to its original form. According to the work from Boulatov's research group,[6] the maximum energy

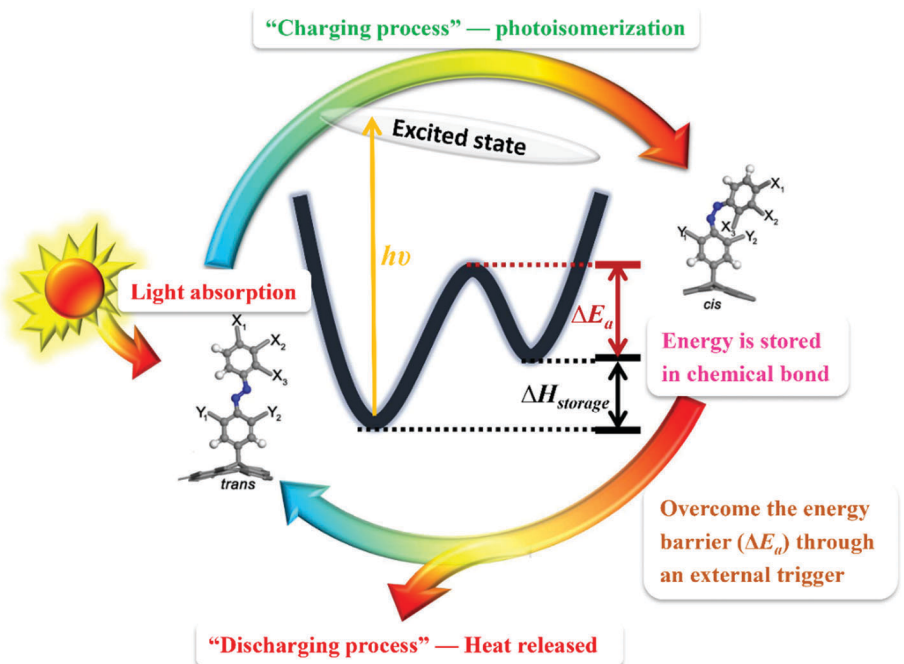

Fig. 3 Schematic illustration of solar thermal conversion and storage mechanism of azobenzene. $\Delta H_{storage}$ is the standard storage enthalpy of *trans*-to-*cis* isomerization, and ΔE_a represents the energy barrier for *cis*-to-*trans* reversion. X_1, X_2, X_3, Y_1, and Y_2 represent different substituents. X_1, X_2, and X_3 are NMe_2, NO_2, COOH, OH, SO_3H, or Cl. Y_1 and Y_2 are NHMe, NO_2, OMe, OEt, F, or Cl.

(ΔG^0_{isom}) that can be stored for any period of time per mole of chromophore must satisfy eqn (1):

$$\Delta G^0_{isom} = \Delta G^{\ddagger}_{isom} + RT \ln \frac{h \ln 2}{\tau_{1/2} k_B T} = \Delta G^{\ddagger}_{isom} - \Delta G^{\ddagger}_{rev} \quad (1)$$

where $\Delta G^{\ddagger}_{isom}$ is the activation free energy for the stable to metastable isomer conversion, $\Delta G^{\ddagger}_{rev}$ is the free energy of activation for thermal reversion of the metastable isomer to the stable isomer, $\tau_{1/2}$ is the time during which half of the stored energy is dissipated spontaneously (half-life). T is the storage temperature, and R, h, and k_B are the gas constant, Planck's constant, and Boltzmann constant, respectively. In this review, the storage enthalpy $\Delta H_{storage}$ is used to characterize the maximum energy that can be stored per mole of azobenzene. ΔE_a is used as the energy barrier for thermal reversion of the metastable (*cis*) isomer to the stable (*trans*) isomer.

2.2 Measurement of solar thermal energy storage

The most frequently used thermal analysis technique for measuring the solar thermal energy storage, *i.e.*, the ΔH of azobenzene photoswitches, is differential scanning calorimetry (DSC). DSC measures the differences in heat flow when a sample absorbs or releases heat due to the thermal effect. The observed heat flows were converted to ΔH using eqn (2):[78]

$$\Delta H = \frac{qM\chi_{cis}}{m}, \quad (2)$$

where q is the heat released (J), as determined by the integration of the DSC signal, m is the mass of the sample, M is the (effective) molecular weight of azobenzene, and χ_{cis} is the mole fraction of the *cis* isomers present. Herein, ΔH is the actually measured storage enthalpy of azobenzene derivatives, whose value often shows a difference with the theoretical maximum storage energy $\Delta H_{storage}$.

DSC is known to help determine the enthalpy differences due to the changes in the physical and chemical properties of loaded samples as a function of time or temperature. It should be noted that DSC has already proved to be a powerful tool for probing ED of Azo-STFs as discussed in the following review.

2.3 Critical parameters for Azo-STFs

In general, the performances of solar thermal fuels based on azobenzene photoswitches are characterized by three important parameters, energy storage density, energy storage half-life, and solar energy conversion efficiency, which are described below.

Energy density (ED) and power density (PD). ED could be considered as the most crucial indicator in the design of a practical high-energy density STF system, which reflects the capability of energy storage. ED can be expressed in several ways, including the mole-energy density (kJ mol^{-1}), mass-energy density (kJ kg^{-1} or W h kg^{-1}), and volume-energy density (kJ L^{-1} or W h L^{-1}).

Power density (PD) refers to the average power density delivered by a fully charged *cis*-Azo as it discharges (*i.e.*, the heat release rate) during the isothermal discharge of *cis*-Azo. Since the effective volume is sensitive to solvation conditions, we usually consider PD per mass (W kg^{-1}). The relation between PD and ED is given by eqn (3):

$$PD = \frac{ED}{T}, \quad (3)$$

where T is the time in which *cis*-Azo fully releases its heat and converts into *trans*-Azo.

Energy storage half-life. Half-life ($\tau_{1/2}$) refers to half the time required by the *cis* isomer to spontaneously convert into the *trans*-isomer. The half-lives of azobenzene and its derivatives can range from minutes to hours and even to days. Besides, the half-life is strongly dependent on the energy barrier of *cis*-to-*trans* reversion. A *cis*-Azo with a short half-life is undesirable as an ideal STF because the short-lived *cis*-Azo needs an intense light source to preserve a sizable fraction of the *cis*-isomer in the photostationary state. Thus, the utility of an Azo-STF is contingent on not only its energy density, but also its half-life in the photostationary state.

Solar energy conversion efficiency. The solar energy conversion efficiency is highly dependent on the isomerization degree of azobenzene, fraction of the *cis*-Azo in the photostationary state, and the photon absorption efficiency. For the photochemical reaction of azobenzene, the solar energy storage efficiency (η) is defined by eqn (4):[78]

$$\eta = \frac{\Delta H_{cis-trans}}{E_{h\nu}} \cdot \frac{\int_{\lambda_1}^{\lambda_2} I(\lambda)\eta_{abs,trans}(\lambda)\phi_{trans\rightarrow cis}(\lambda)d\lambda}{\int_{\lambda_1}^{\lambda_3} I(\lambda)d\lambda} \quad (4)$$

where $\Delta H_{cis-trans}$ is the enthalpy difference between the metastable (*cis*) and stable (*trans*) azobenzene isomers. $E_{h\nu}$ is the energy of the photons of absorbed light. The limit λ_1 is either the lower limit of the UV-vis absorption data for the *trans*-Azo or the lower limit of the solar spectral irradiance data (ASTM G173-03). The limits λ_2 and λ_3 are the upper limits for the UV-vis absorption spectrum for the stable (*trans*) isomer and the upper limit of the solar spectra irradiance data, respectively. The term $\eta_{abs,trans}(\lambda)$ is the wavelength-dependent efficiency of absobance of the stable isomer, and $\phi_{trans\rightarrow cis}(\lambda)$ is the wavelength-dependent quantum yield for *trans* → *cis* photoisomerization. It should be noted that eqn (4) is evolved from the calculation of solar energy storage efficiency for a photochemical reaction A → B, which was firstly determined by Bren *et al.*[64] Besides, the maximum energy conversion efficiency of Azo-STFs tends to be somewhat lower than that of silicon photovoltaics.[122] This implies that there is much room for improvement in the solar energy conversion efficiency of Azo-STFs.

3. Advances in azobenzene materials for solar thermal fuels

Until now, a variety of azobenzene derivatives have been designed toward the promising applications of STFs. Although no reported system has fully met the strict requirements yet, researchers have already proposed many useful routes for developing various functionalized azobenzenes including pure

azobenzene derivatives, nanocarbon-templated azobenzenes, and polymer-templated azobenzenes. In this section, we present examples of representative Azo-STFs reported in the literature, focusing on the improvement in STF performance by different molecular design engineering. It is expected that such an in-depth review could inspire the researchers for molecular design towards efficient Azo-STFs.

3.1 Solar thermal fuels based on azobenzene derivatives

In 1978, Adamson *et al.* firstly determined the storage enthalpy ($\Delta H_{storage}$ = 49 kJ mol^{-1} or 269 J g^{-1} or 75 W h kg^{-1}) of azobenzene.[123] The half-life of *cis*-Azo was reported to be 4.2 days. Olmsted and co-workers investigated the potential for the storage of solar energy by substituted azobenzenes.[102] However, they concluded that azobenzenes were unfavorable for photochemical solar energy storage because of rapid thermal reversion rates and limited solubilities in polar solvents. Unless the azobenzene solution is stored in a cool and dark room, the *cis*-azobenzene would release heat at high temperature. By taking such precautions, long-term storage and repeated usage of Azo-STFs can be achieved.[103]

Molecular azobenzene has encountered immense challenges in the field of solar thermal storage. To override these hurdles, a liquid azobenzene derivative (**1**) as a solvent-free STF was developed by Kimizuka and co-workers.[124] A branched 2-ethylhexyl group was introduced in the *para*-position of azobenzene *via* an ether bond to fluidify the resulting azobenzene at room temperature (Fig. 4a). It should be noted that the molecular weight of the 2-ethylhexyl group was so small that it could achieve condensed-phase photoisomerization while maintaining a relatively high energy density. After UV irradiation, the compound undergoes a *trans*-to-*cis* photoisomerization with the color change from bright orange to dark red (Fig. 4b). Fig. 4c shows the typical photoisomerization behavior of azobenzene photoswitches, wherein the peaks at around 344 nm and 443 nm could be assigned to π–π* and n–π* absorptions, respectively. Fig. 4d shows the DSC curves of *cis*-Azo **1** with different photoisomerization degrees. In the DSC curve, the exothermic peaks can be observed at around 120 °C, and the energy density was calculated as 35 kJ mol^{-1} (113 J g^{-1} or 32 W h kg^{-1}) for a *cis*-Azo content of 68%. Furthermore, the *cis*-to-*trans* isomerization enthalpy is linearly dependent on the molar content of *cis*-Azo. By extrapolating the plot, the ΔH value corresponding to 100% *cis*-Azo was calculated as 52 kJ mol^{-1} (168 J g^{-1} or 47 W h kg^{-1}) (Fig. 4e). This study demonstrated that a liquid azobenzene derivative with low-molecular weight could be considered a new potential candidate for molecular solar thermal storage materials. Nevertheless, challenges such as limited exothermicities, short half-life, and difficulty in obtaining pure *cis*-isomers remain.

To overcome the above-mentioned limitations, Grossman's research group reconsidered the design of pure azobenzene derivatives for solid-state applications. To obtain tunable solid-state STFs, bulky aromatic groups such as biphenyl, phenyl, and *tert*-butyl phenyl were grafted onto azobenzene derivatives (Fig. 5a, **2a–c**).[125] Due to repulsion and steric hindrance, the introduction of bulky phenyl groups would elevate *cis*-Azo to a higher energy state, thus increasing the energy difference between the *trans* and *cis* forms. Apart from increasing the energy density, the addition of such groups to azobenzene promotes the formation of a solid-state molecular film. Fig. 5b shows the excellent thermal stability of the azobenzene molecular

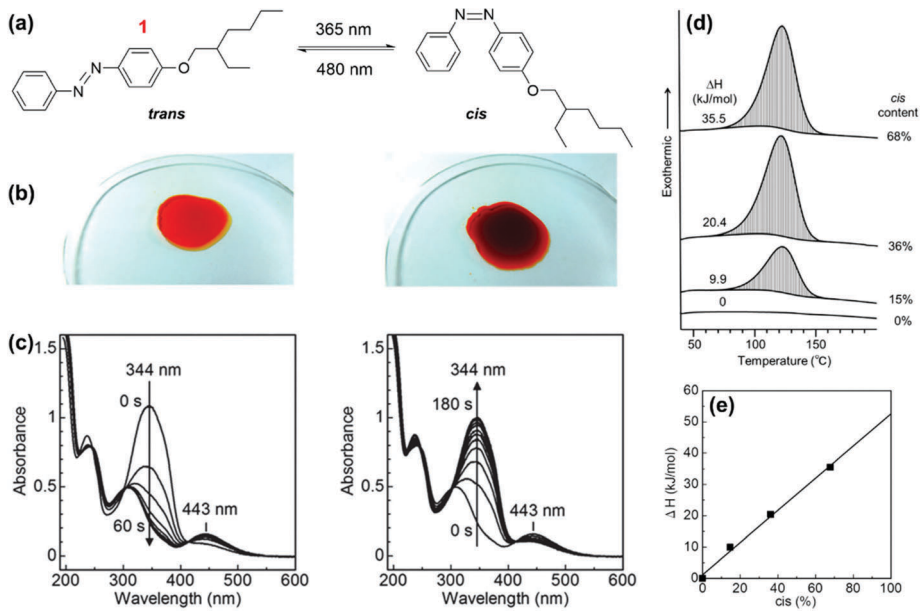

Fig. 4 (a) Molecular structure and photoisomerization processes of liquid azobenzene derivative **1**. (b) Pictures of azobenzene derivative **1** in *trans* and *cis* states. (c) UV-vis absorption spectra of liquid azobenzene derivative **1** under certain conditions under UV (365 nm) and visible-light (480 nm) irradiation. (d) DSC curves of *cis*-Azo **1** at different molar ratios. Heating rate is 50 K min^{-1}. (e) Dependence of *cis*-to-*trans* isomerization enthalpy, ΔH, on the molar content of the *cis*-isomer. Reprinted with permission from ref. 124. Copyright 2014 Royal Society of Chemistry.

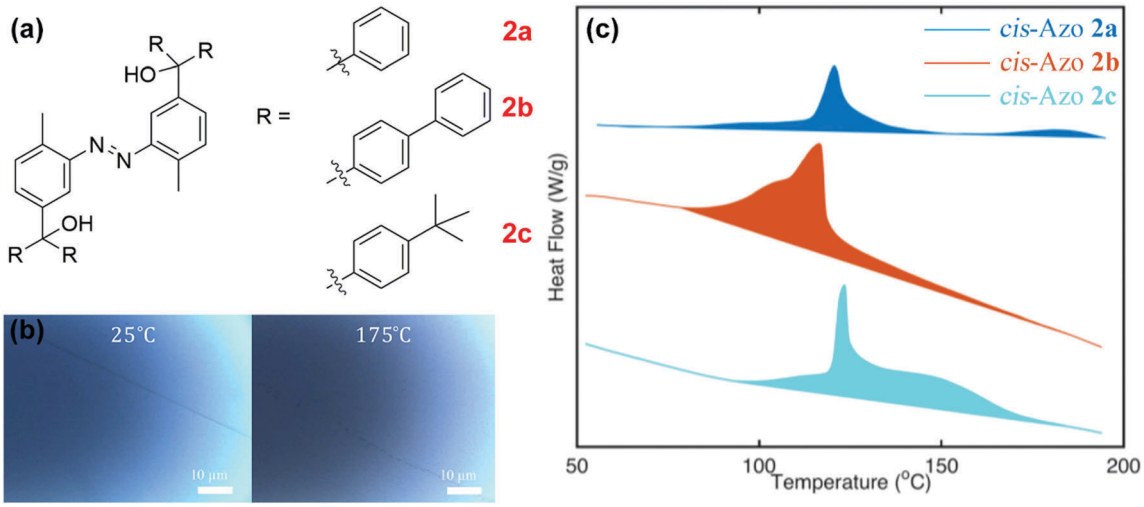

Fig. 5 (a) Molecular structure of bulky phenyl group-functionalized azobenzene derivatives **2a–c**. (b) Optical images of azobenzene derivative **2c** films on silicon at 25 °C (left) and 175 °C (right). (c) DSC curves of *cis*-azobenzene derivatives **2a–c** from top to bottom. The region enclosed with the flat baseline represents the area integrated to obtain energy release. Reprinted with permission from ref. 125. Copyright 2017 American Chemical Society.

thin film. It was found that the addition of bulky phenyl groups could effectively prevent the π–π stacking of the azobenzene derivative under thermal annealing conditions. Fig. 5c shows the DSC curves of three azobenzene derivatives in the *cis* form. The energy density of heat release in a single molecule of **2a–c** is 77 kJ mol^{-1} (134 J g^{-1} or 37 W h kg^{-1}), 88 kJ mol^{-1} (100 J g^{-1} or 28 W h kg^{-1}) and 87 kJ mol^{-1} (108 J g^{-1} or 30 W h kg^{-1}), respectively. These data are also given in Table 2. It is noteworthy that the DSC curves do not show a smooth peak, which may be ascribed to the difference in the activation energies of different grafted functional groups caused by the differences in the local environment. This study revealed that structural engineering of pure azobenzene molecules is an effective pathway to obtain high-energy density and thermally stable molecular Azo-STFs.

Most recently, the combination of azobenzene and other heat storage materials has provided some inspiration for the design of novel molecular Azo-STFs. Grossman and co-workers have reported light-controlled thermal energy storage materials, which consist of azobenzene molecules (**3**) and organic phase-change materials (PCM), *i.e.*, tridecanoic acid, as shown in Fig. 6a.[126] Fig. 6b shows light-controlled thermal energy storage and release cycle. Firstly, the crystalline composite (solid-PCM + *trans*-Azo, Fig. 6b, **i**) absorbed external thermal energy. When the temperature reached its melting point (T_m, 43 °C), the crystalline composite converted into a mixture of liquid PCM and crystalline aggregates of the azobenzene dopant (Fig. 6b, **ii**). Then, UV irradiation enabled the conversion of *trans*-Azo dopants to its *cis* conformation, rendering them well dispersed in the liquid PCM (Fig. 6b, **iii**). Finally, the liquid state of the composite (liquid-PCM + *cis*-Azo) was sustained by subsequently cooling to a temperature below the original crystallization temperature (T_c, 38 °C). In the meantime, the stored latent thermal energy was fully maintained (Fig. 6b, **iv**). The photographs in Fig. 6c show the different stages of azobenzene-doped PCM composites, which are in accordance with the schematic cycle shown in Fig. 6b. These results indicated that the azobenzene-doped PCM composites could sustain the stored latent heat even when the temperature was decreased. Besides, the T_c values of the uncharged (PCM + *trans*-Azo) and charged (PCM + *cis*-Azo) composites were measured by DSC (Fig. 6d). For the uncharged composite, the first exothermic peak appeared at 48 °C, which can be ascribed to the crystallization of *trans*-Azo, followed by PCM crystallization at 38 °C. On the other hand, the charged counterpart crystallized at 28 °C, followed by the crystallization of *cis*-Azo at 9 °C. It should be noted in Fig. 6d that the T_c and T_m of pristine *trans*-Azo (60 °C and 73 °C, respectively) significantly decreased for this composite, which is mainly attributed to the solvation effect of the liquid-state PCM. Thus, it can be concluded that the phase-transition temperatures of such azobenzene-doped PCM composites can be varied by adjusting the doping level in the composite and the cooling rate. In this study, the introduction of azobenzene dopants into conventional organic PCMs not only allowed the PCMs to change the intermolecular dynamics and provide stability to the phase storing thermal energy, but also rendered them optically controllable for energy release. This technology could retain the thermal energy of ~200 J g^{-1} in the materials for more than 10 h at temperatures below the original crystallization point. This result implies that the azobenzene dopants can be locked in the liquid phase of PCMs as a result of reducing their crystallization temperature by tuning the doping level in the composite and the cooling rate, and thus the thermal energy was kept at a lower temperature. This approach unlocks numerous opportunities for portable thermal energy storage systems.

Table 1 summarizes the ED and half-lives of pure azobenzene derivatives for STF applications. Initially, azobenzene derivatives were considered unsuitable for energy storage because of their short half-lives. However, with increasing necessity for

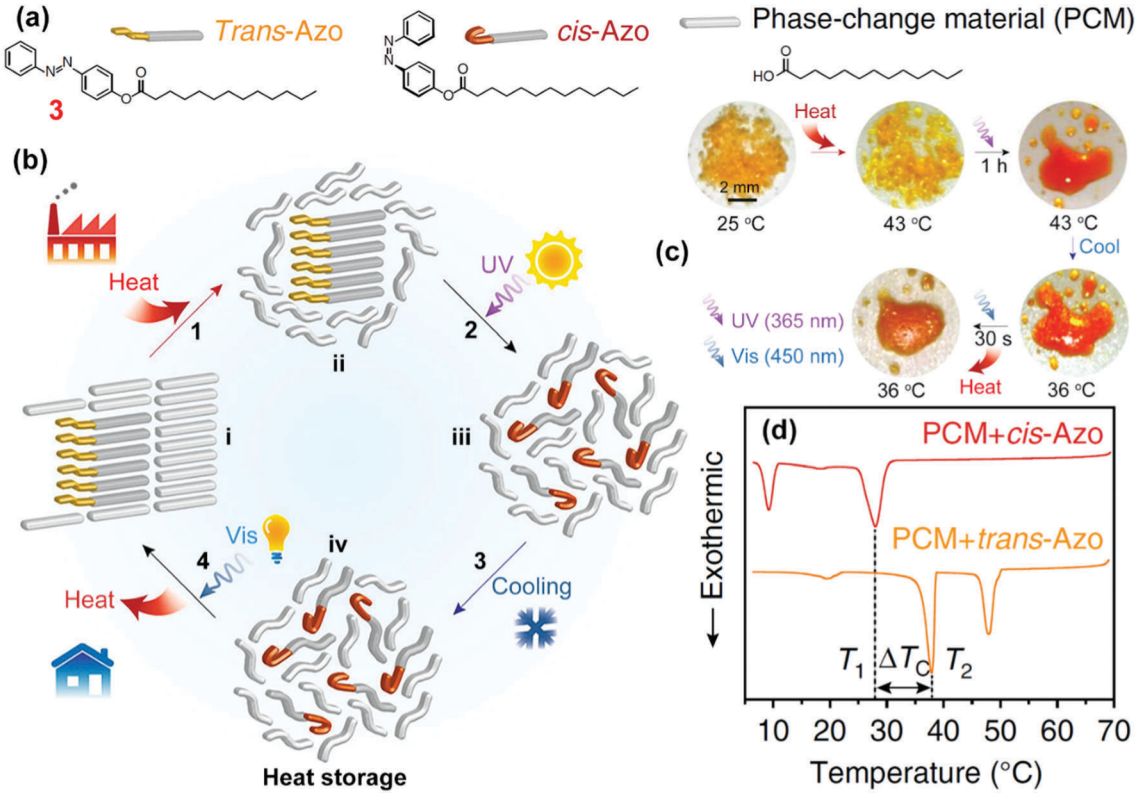

Fig. 6 (a) Chemical structures of azobenzene dopant and PCM (tridecanoic acid). (b) Schematic of light-operated thermal energy storage and release cycle, including heat absorption of the PCM composite (**1**), UV irradiation leads to photoisomerization of azobenzene dopants (**2**), cooling of the liquefied PCM composite (**3**), and visible-light drives the reverse isomerization and heat release (**4**). The straight and curved rods exhibit different degrees of translational and rotational freedom, *i.e.*, phase **i** represents solid-PCM + *trans*-Azo (25 °C), phase **ii** represents liquid-PCM + *trans*-Azo (43 °C), phase **iii** represents liquid-PCM + *cis*-Azo (43 °C), and phase **iv** represents liquid-PCM + *cis*-Azo (36 °C), respectively. (c) Corresponding photographs of azobenzene-doped PCM composites during solid-state heat absorption, UV charging, cooling, visible-light-induced discharging, and heat-release processes. (d) DSC curves of charged and uncharged azobenzene-doped PCM composites obtained while cooling from 70 °C at a rate of 5 °C min^{-1}. T_1, T_2, and ΔT_c denote different crystallization points and the gap, respectively. Reprinted with permission from ref. 126. Copyright 2017 Nature Publishing Group.

solid-state integration of small molecules for functional devices, molecular thin films have attracted tremendous attention because of their versatility, ease of processing, and cost reduction. To date, much efforts, including computational[26,128] and experimental, have been devoted to improving the performance of molecular Azo-STFs. As can be seen in Table 1, the grafting of functional groups on unsubstituted Azo increased the energy density by 80%. These results suggest that appropriate

Table 1 Parameters related to azobenzene derivative STFs

Azo-based molecules	Energy density (kJ mol^{-1})	(J g^{-1})	(W h kg^{-1})	$\tau_{1/2}$	State	Ref.
Azobenzene	49	269	75	100.0 h	Liquid	102 and 127
4,4′-Dimethoxy Azo	80	331	92	9.6 h	Liquid	28
2,2′-Dimethoxy Azo		[a]		168.0 h	Liquid	28
2,2′-Diethyl Azo		[a]		33.6 h	Liquid	28
2,6,2′6′-Tetramethyl Azo		[a]		108.0 h	Liquid	28
3-Nitro-4′-dimethylamino Azo	98	350	97	14.4 min	Liquid	28
2,6-Dimethyl-4-methoxy-4′-nitro Azo	30	95	26	1.9 h	Liquid	28
Methyl orange	94	287	80	57.6 min	Liquid	28
1	35	113	32	[b]	Liquid	124
2a	77	134	37	[b]	Liquid ↔ solid	125
2b	88	100	28	[b]	Liquid ↔ solid	125
2c	87	108	30	[b]	Liquid ↔ solid	125
3	[b]	200	56	10 h	Liquid ↔ solid	126

[a] Cannot be reliably determined owing to low quantum yield. [b] No data were found in the references.

molecular engineering of azobenzene could be a valid tactic for designing solid-state STFs.

3.2 Solar thermal fuels based on nanocarbon-templated azobenzene

Although the molecular engineering of azobenzene photoswitches could improve the energy storage property of STFs, some obstacles such as short half-life and limited exothermicities need to be addressed. To circumvent these challenges, Grossman's research group recently developed a set of novel Azo-STFs, where azobenzene photoswitches were bound to different robust carbon-based templates such as graphene, carbon nanotubes (CNT), and C_{60} (Fig. 7a).[129,130] Using first-principles calculations, they predicted that these STFs could reversibly store solar energy with densities comparable to Li-ion batteries, potential external efficiencies of up to 35%, and tunable thermal stability from minutes to years.[129] As shown in Fig. 7b, compared with the systems using unsubstituted azobenzene, the key fundamental properties of nanocarbon-templated Azo-STFs could be coordinated over a large extent by utilizing carbon templates with diverse geometries and electronic properties. It is anticipated that templated azobenzenes using carbon-based materials could enhance not only the energy densities and storage lifetimes of the resulting STFs, but also the optical and electronic properties, thermal stability, chemical durability, as well as temperature when the thermal back-reaction is triggered.

3.2.1 Carbon nanotube-templated azobenzene. In 2007, our group firstly synthesized a photoactive multiwalled carbon nanotube (MWCNT) by grafting azobenzene onto the sidewalls of MWCNT *via* covalent bonding, as shown in Fig. 8.[131,132] We investigated the polarized optical properties of MWCNT-templated azobenzene composites by UV-vis and photoluminescence spectroscopies. Although the property of solar energy storage was not explored, our study provided a wealth of information to guide the synthesis of CNT-templated azobenzene composites. In 2011, Grossman and co-workers theoretically demonstrated that the azobenzenes chemically linked with carbon nanotube (CNT) enabled the formation of highly ordered and closely packed arrays, thus increasing both the storage half-life and energy density of the resulting STFs due to the specific chemical interactions between the neighboring azobenzene molecules.[133] Compared to individual azobenzene molecules, the presence of CNT matrices could break the molecular symmetry of azobenzene, imposing a close-packed crystalline-like state to prevent the isomerization reaction *via* rotation of phenyl rings, thus increasing the potential phase space for the formation of H-bonds. As shown in Fig. 9a, several azobenzene derivatives with different numbers of hydroxyl substituents on phenyl rings were introduced on the CNT to tune the relative stability of the two isomers *via* the addition of H-bonds. The calculation results showed that the different numbers of molecular H-bonds in *trans*- and *cis*-Azo on the surface of the CNT resulted in a significant increase in ΔH and $\tau_{1/2}$. Generally, hybrid structures with more H-bonds and/or stronger (shorter) H-bonds are more stable. Hence, a larger ΔH could be achieved by maximizing the number of H-bonds in the *trans* state while minimizing the H-bonds in the *cis* state. In addition, the stability of both *trans* and *cis* configurations increased due to the formation of H-bonds, leading to a relatively long half-life. Furthermore, Fig. 9b shows several possible patterns for CNT-templated dihydroxy azobenzene derivatives, and it was found that the strength and the number of H-bonds in the *trans* and *cis* configurations are closely related to the relative positions of two OH groups. In short, the crystalline-like structure provides two key improvements: (i) an increase in volume density due to the packing of the photomolecule per volume compared to the solution of free molecules, and more importantly, (ii) the ordered arrangement in close proximity and steric interactions

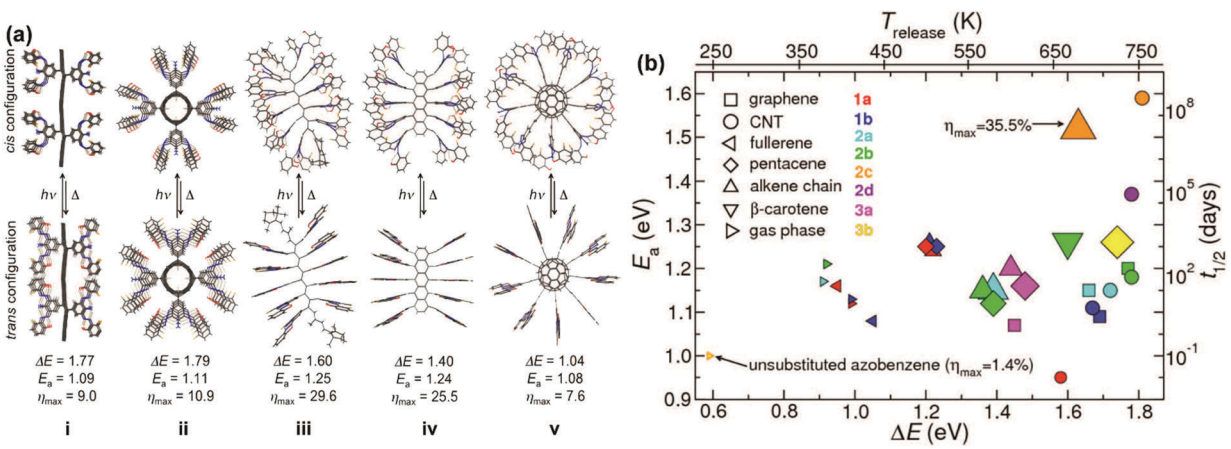

Fig. 7 (a) Calculated *trans* and *cis* configurations and properties of nanocarbon-templated azobenzenes including graphene-templated azobenzene (i), CNT-templated azobenzene (ii), β-carotene-templated azobenzene (iii), pentacene-templated azobenzene (iv), and C_{60}-templated azobenzene (v). Orange, red, blue, dark gray, and white balls/sticks represent F, O, N, C, and H atoms, respectively. (b) Calculated thermal activation barrier (E_a) *vs.* stored energy per molecule (ΔE) for nanocarbon-templated azobenzene and gas phase azobenzene derivatives. The alternate axes indicate half-life ($\tau_{1/2}$) and temperature of the released heat ($T_{release}$), estimated from E_a and ΔH, respectively. The size of the symbols illustrates the relative values of the maximum external efficiency (η_{max}). Reprinted with permission from ref. 129. Copyright 2013 AIP Publishing.

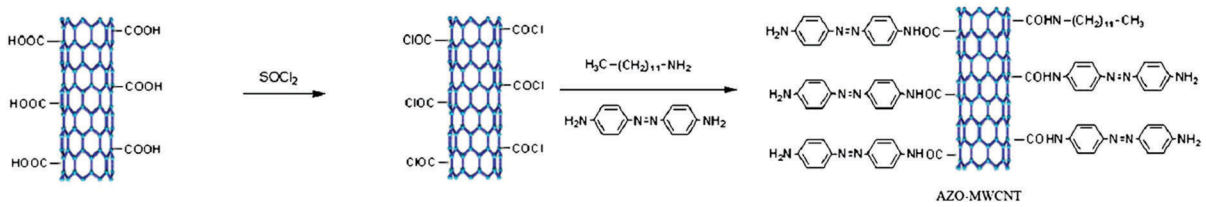

Fig. 8 Synthesis route to Azo-MWCNT. Reprinted with permission from ref. 132. Copyright 2007 AIP Publishing.

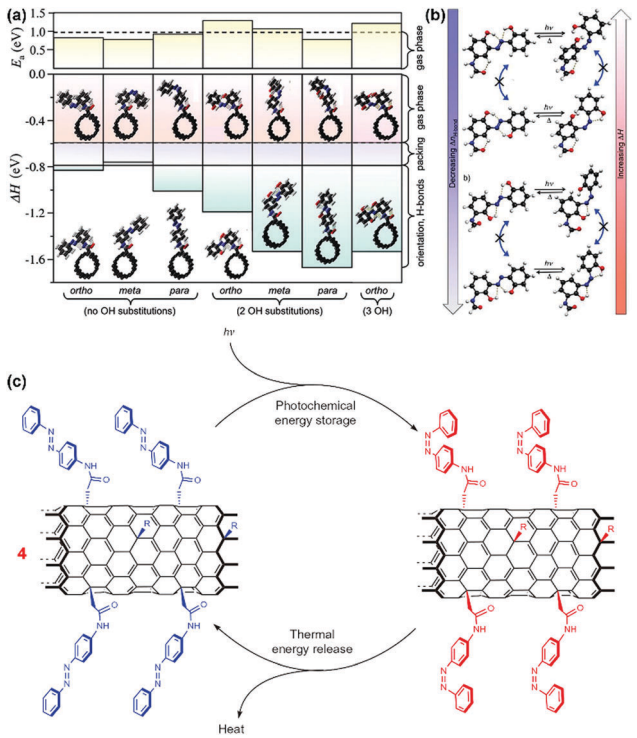

Fig. 9 (a) Density functional theory calculation values of ΔH and E_a for a typical sample of CNT-templated azobenzene systems. (b) Hydrogen bonding effects. The *cis* and *trans* isomers of several possible dihydroxy azobenzene molecules bound to a CNT substrate *via* an attachment at the *meta*-position. (a) and (b) Reprinted with permission from ref. 133. Copyright. 2011 American Chemical Society. (c) Reaction scheme for photochemical energy storage and thermal energy release in CNT-templated azobenzene systems. Reprinted with permission from ref. 78. Copyright 2014 Springer Nature.

enable new ways to design the inter- and intra-molecular bonding, leading to an increase in storage capacity.

In 2014, Grossman's research group turned the theoretical model of CNT-templated azobenzene hybrids into reality (see in Fig. 9c).[78] An energy density of 120 kJ mol^{-1} ($\sim$200 J g^{-1}, or $\sim$56 W h kg^{-1}) was achieved in the CNT-templated azobenzene, whereas an energy density of 58 kJ mol^{-1} ($\sim$160 J g^{-1}, or $\sim$44 W h kg^{-1}) was observed in non-templated azobenzene. Such CNT-templated azobenzene systems display an obvious improvement in the energy stored per molecule while maintaining excellent cyclability and stability. It should be noted that the composite materials reported here did not cover the inter- and intra-molecular H-bonds, which was proposed in their theoretical model. In this research, the authors believed that interactions between azobenzene and the neighboring templates could be more important than those with an individual template.

3.2.2 Graphene-templated azobenzene. Despite the great progress in CNT-templated azobenzene hybrids, simultaneous improvement of ΔH and $\tau_{1/2}$ by optimizing molecular structures of azobenzene remains a challenging task because the intermolecular interactions between two azobenzene molecules on a carbon nanostructure template are closely related to a specific steric configuration, a suitable intermolecular distance, and substituent groups on the phenyl ring. Alternatively, graphene, a two-dimensional sheet with sp^2-hybridized carbon atoms arranged in a hexagonal lattice, presents remarkable potential for optoelectronic devices because of its unique optical, mechanical, and electronic properties.[134] Graphene produces no impurities during growth, which enables its facile fabrication directly on the substrate without purification processes and complicated separation. Graphene oxide (GO) is an isolated monoatomic membrane of carbon containing functional groups such as epoxide, carboxyl, and hydroxyl. These functional groups provide opportunities for tailoring the properties of graphene by changing the addends. For example, an optically tunable electronic property could be achieved by attaching a photo-responsive azobenzene molecule on graphene sheets. Interestingly, the photoisomerization reaction can be catalyzed by efficient charge transfer between azobenzene and graphene.[130,135–138]

Our research group made much effort in optimizing the molecular structure of graphene-templated azobenzene hybrids.[64] Firstly, we constructed a series of models of graphene-templated azobenzene hybrids, in which the photo-responsive azobenzene with various functional groups at different positions (*ortho*-, *meta*- and *para*-) was covalently bound to graphene.[139] Density functional theory calculations predicted that the intermolecular distance between two adjacent azobenzene molecules on graphene, the electronic interaction, steric hindrance, and inter- or intramolecular H-bonds lead to a change in $\Delta H_{storage}$. Thus, we considered that the 2D graphene nanosheet is an ideal platform to support the nanocarbon-templated Azo-STFs. Based on the calculations, a series of graphene-templated azobenzene materials have been designed and successfully synthesized by our research group, as shown in Fig. 10.[139–144] We focused on enhancing the energy density and half-life through several efficient methods such as increasing the number of molecular interactions, improving the grafting density, optimizing the steric configuration, and attaching suitable substituents to different positions of azobenzene.

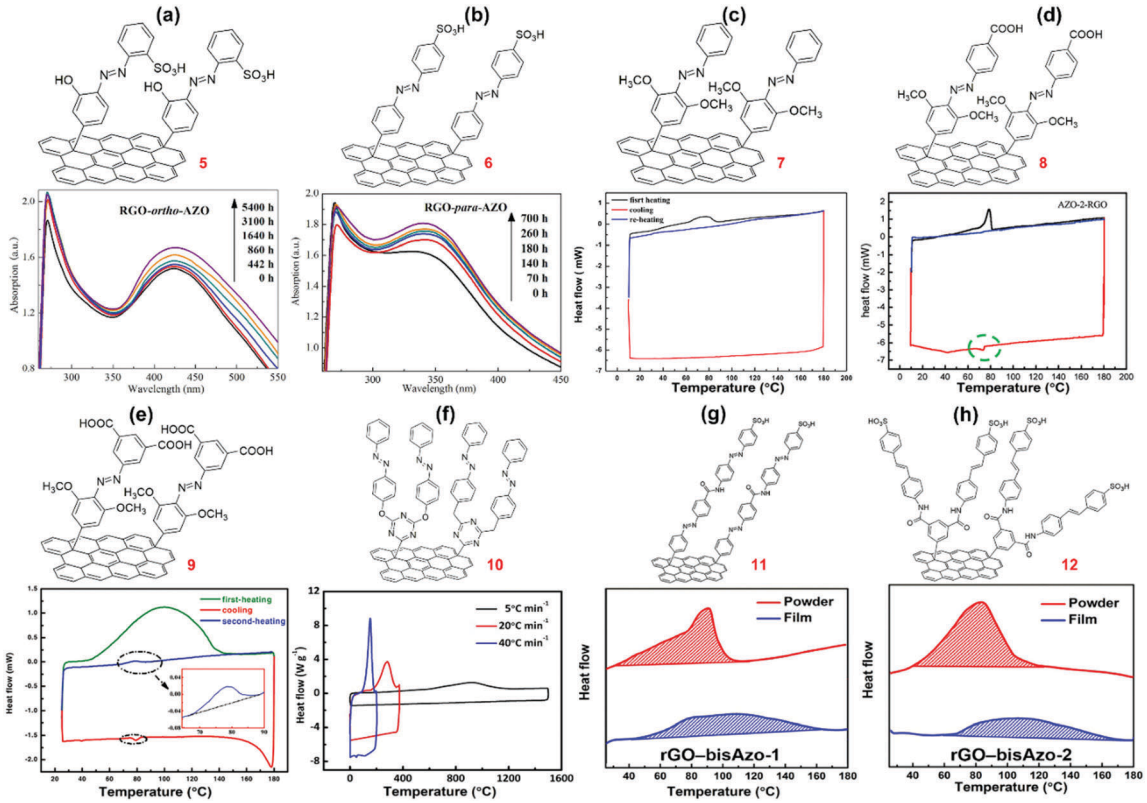

Fig. 10 (a and b) Chemical structures and time-evolved absorption spectra of RGO–*ortho*-Azo and RGO–*para*-AZO hybrids. Reprinted with permission from ref. 140. Copyright 2013 Springer Nature. (c–f) Chemical structures and DSC curves of RGO–*ortho*-Azo, RGO–*para*-AZO, and RGO–bis-Azo hybrids. (c) and (d) Reprinted with permission from ref. 141. Copyright 2015 Royal Society of Chemistry. (e) Reprinted with permission from ref. 142. Copyright 2015 Royal Society of Chemistry. (f) Reprinted with permission from ref. 143. Copyright 2016 Royal Society of Chemistry. (g and h) Chemical structures and DSC curves of the first heating stage of RGO–bis-Azo-1 and RGO–bis-Azo-2. Reprinted with permission from ref. 144. Copyright 2017 Wiley-VCH.

Furthermore, we reported reduced graphene oxide-templated azobenzene hybrids (RGO–Azo) *via* covalent functionalization.[140] The $\Delta H_{storage}$ and $\tau_{1/2}$ were improved by intermolecular H-bonds, which were controlled by the substitution (*ortho* or *para*) and close-packing arrays of azobenzene on RGO. As shown in Fig. 10a and b, RGO–*ortho*-Azo exhibited a longer half-life (**5**, 5400 h) than RGO–*para*-Azo (**6**, 116 h), whereas RGO–*para*-Azo showed a high ED of 75 W h kg^{-1} than RGO–*ortho*-Azo (42 W h kg^{-1}). In order to gain a deep understanding of the relationship between ED, graft density, and intermolecular H-bond, we designed three RGO–Azo hybrid materials with methoxyl and/or carboxyl groups on the *ortho*- (*meta*- or *para*-) position of azobenzene, as shown in Fig. 10c–e (**7**–**9**).[141,142] According to the characterization of thermal stability and chemical structure, every 16–19 carbon atoms of RGO supported one azobenzene molecule. Such close-packed and highly grafted azobenzene–graphene hybrids capacitate the formation of intermolecular H-bonds in both *trans* and *cis* forms of azobenzene. In the meantime, the two neighboring *trans*-Azo formed two intermolecular H-bonds in the form of OH$\cdots$O, and *cis*-Azo formed only one H-bond (Fig. 11a). The difference in the numbers of intermolecular H-bonds between *trans*- and *cis*-Azo resulted in a large enthalpy difference, which led to the improvement in ED and half-life. As shown in Fig. 11b, we considered that H-bonding interactions not only occurred between the two adjacent azobenzenes on the same graphene nanosheets, but also between two azobenzenes on adjacent graphene nanosheets. Furthermore, the DSC curve generated from the second-heating cycle indicated the existence of molecular H-bonds (Fig. 10d and e). These studies indicated that optimizing the molecular structure and steric configuration of azobenzene on the graphene template is very important to facilitate the isomerization and intra/intermolecular interaction.

Most recently, our group presented three templated assemblies of close-packed bis-azobenzene (bis-Azo) covalently grafted onto RGO ((**10**–**12**) in Fig. 10f–h and 12).[143,144] Theoretically, the intramolecular coupling of the bis/tri-Azo not only lowers the energy of the *trans*-isomer, but also stabilizes the *cis*-isomer due to the large steric hindrance.[145,146] The experimental setup as schematically illustrated in Fig. 12a was used to investigate the closed cycle of UV light harvesting, storage in darkness, and heat release in the solid-state films. Fig. 12b and e show the difference in temperature between UV-irradiated and unirradiated films. The continuous heat release led to an increase in the temperature of UV-irradiated RGO–bis-Azo films, which was higher than that of the unirradiated film. As can be seen in Fig. 12c–g, the RGO–bis-Azo-2 film exhibits a maximum temperature difference of 15 °C, releasing 85% of the heat

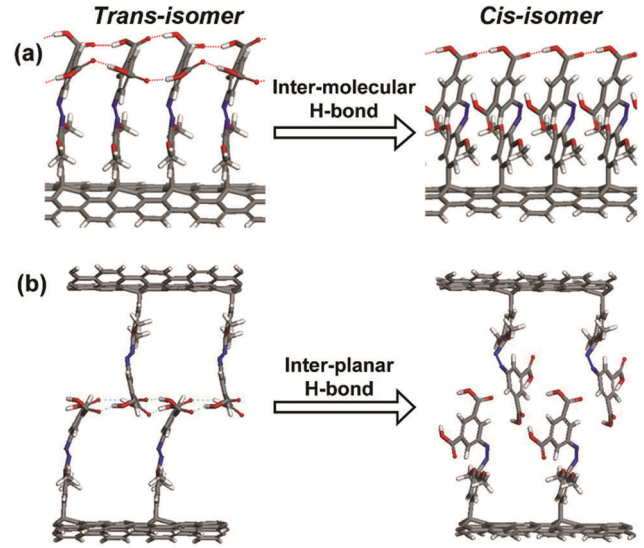

Fig. 11 Illustration of inter-molecular H-bond interaction (a) and inter-planar bundling (b) of high-grafting density RGO-templated azobenzene hybrids. Reprinted with permission from ref. 142. Copyright 2015 Royal Society of Chemistry.

in 8 min (60–140 °C). The result indicated that solid-state RGO–bis-Azo films exhibited a remarkable photothermal effect and excellent cycling, which could be used for energy storage by controlling the heat release and optimizing the molecular interactions. These solid-state heat-release graphene-templated azobenzene hybrids pave the way for the development of highly efficient and high-energy STFs for a multitude of applications.

Table 2 summarizes the EDs, half-lives, and grafting densities of nanocarbon-templated azobenzene STF materials. The following conclusions can be drawn from Table 2: (i) the ED increases along with grafting density. However, the grafting density is restricted by the decrease in reactivity, steric hindrance of azobenzene, and the stacking of nanosheets. (ii) The substituents of azobenzene and the intermolecular H-bonds in both *trans*-Azo and *cis*-Azo lead to a robust increase in the ED and half-life. (iii) Compared to a single azobenzene, the bis-Azo molecule displays a higher ED and a longer half-life. Despite our focus on azobenzene photoswitches and carbon-based templates in the mentioned studies, these experimental results strongly suggest that the same principles can be employed to design efficient STFs based on other molecular photoswitches and templated materials.

3.3 Solar thermal fuels based on polymer-templated azobenzene

Polymer-templated azobenzenes could form uniform and flat films with controllable thicknesses and display feasibility for the application of large-area heat release. The uniform Azo-polymer films help in capturing photons, and heat release could occur in the solid-state as well as *via* controlling their *cis*-to-*trans* isomerization, which provides the opportunity of integrating STF materials into numerous existing heating devices. Fortunately, in the past few decades, scientists have maintained considerable research enthusiasm for the interesting properties of polymer-templated azobenzenes, such as photoinduced phase transition, photoinduced birefringence and dichroism, optical nonlinearities, and photocontrolled reversible property changes.[147] As a result, a large amount of photoactive polymer-templated azobenzenes have been developed, which allows us to explore this rapidly developing field more conveniently. Therefore, polymer-templated azobenzenes serving as STF materials have aroused considerable research interest.

3.3.1 Solid-state Azo-STFs. Recently, Grossman *et al.* designed a simple polymer, in which the main chain consists of an alkyl

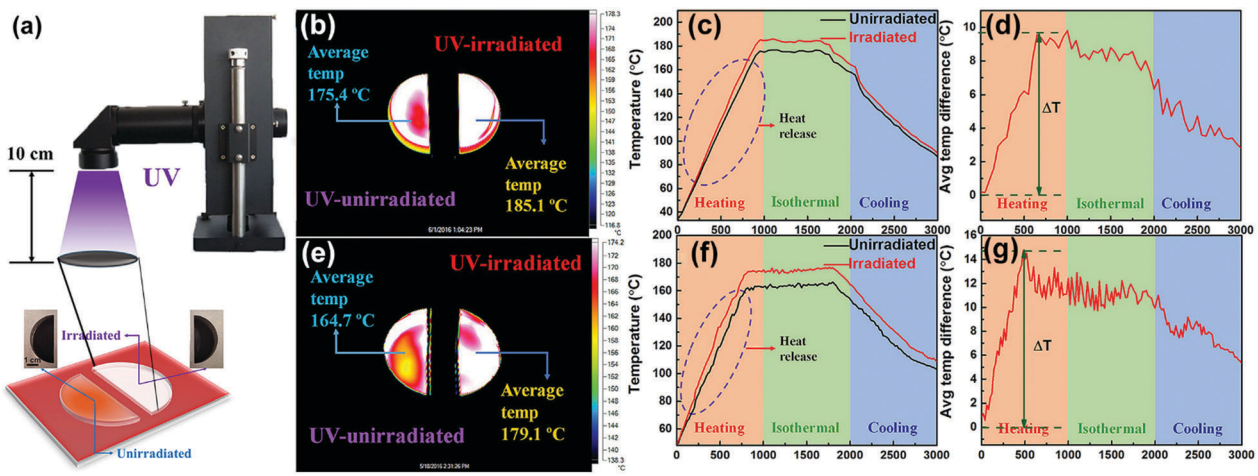

Fig. 12 (a) Schematic illustration of the experiment using a heating stage with controllable temperature: half of the film was irradiated with UV light and the other half was left in darkness. (b and e) Top-view IR heat map of RGO–bis-Azo films (**11** and **12**) with and without UV irradiation. Each uniform RGO–bis-Azo film was cut into half. The heat maps show the maximum rising temperature between areas; the color bar indicates the relative magnitude of the heat released. Average temperatures of (c) RGO–bis-Azo-1 and (f) RGO–bis-Azo-2. Average difference in temperatures of (d) RGO–bis-Azo-1 and (g) RGO–bis-Azo-2. Reprinted with permission from ref. 144. Copyright 2017 Wiley-VCH.

Table 2 Parameters related to nanocarbon-templated Azo-STFs

Nanocarbon-templated Azo-STFs	Energy density (kJ mol^{-1})	Energy density (J g^{-1})	Energy density (W h kg^{-1})	$\tau_{1/2}$ (h)	State	Grafting density	Ref.
4	120	200	56	33	Liquid ↔ solid	1/16	78
5	60[a]	151	42	5408	Liquid ↔ solid	1/10	140
6	103[a]	270	75	116	Liquid ↔ solid	1/10	140
7	118	245	68	2	Liquid ↔ solid	1/19	141
8	192	403	112	792	Liquid ↔ solid	1/16	141
9	265	497	138	1248	Liquid ↔ solid	1/17	142
10	318[a]	288	80	1320	Liquid ↔ solid	1/50	143
11	412[a]	346	96	1120	Solid	1/59	144
12	572[a]	472	131	900	Solid	1/46	144

[a] The mole-energy density (kJ mol^{-1}) is calculated through multiplying M_n (g mol^{-1}) and mass-energy density (J g^{-1}), where M_n is the molecular weight of azobenzene compounds.

chain while the azobenzene is the pendant group (Fig. 13a).[148] The materials exhibited relatively long half-lives at room temperature (92 ± 1 h for the monomer and 55 ± 1 h for the polymer). Fig. 13b shows the DSC curves of the monomer (42 ± 2 W h kg^{-1} or 151 J g^{-1}) and polymer (29 ± 2 W h kg^{-1} or 104 J g^{-1}) species after UV irradiation in a toluene solution (charging process). The ED difference between the monomer and polymer may arise from the variations in light absorption efficiency, photoisomerization quantum yield, influence of photostationary state, and thermal reversion barriers.[81] Steric hindrance may restrict photoswitching in the solid state due to the presence of both rotation (steric-sensitive) and inversion mechanisms for isomerization, thus limiting the performance of the STFs.[148–150] Fig. 13c and d show a photograph of a large-area freestanding polymer film obtained by a facile solution spin-coating process. During the spin-coating process, a liquid cross-linking polymer was applied to balance the dissolution of the underlying film. To test the heat release, they designed an

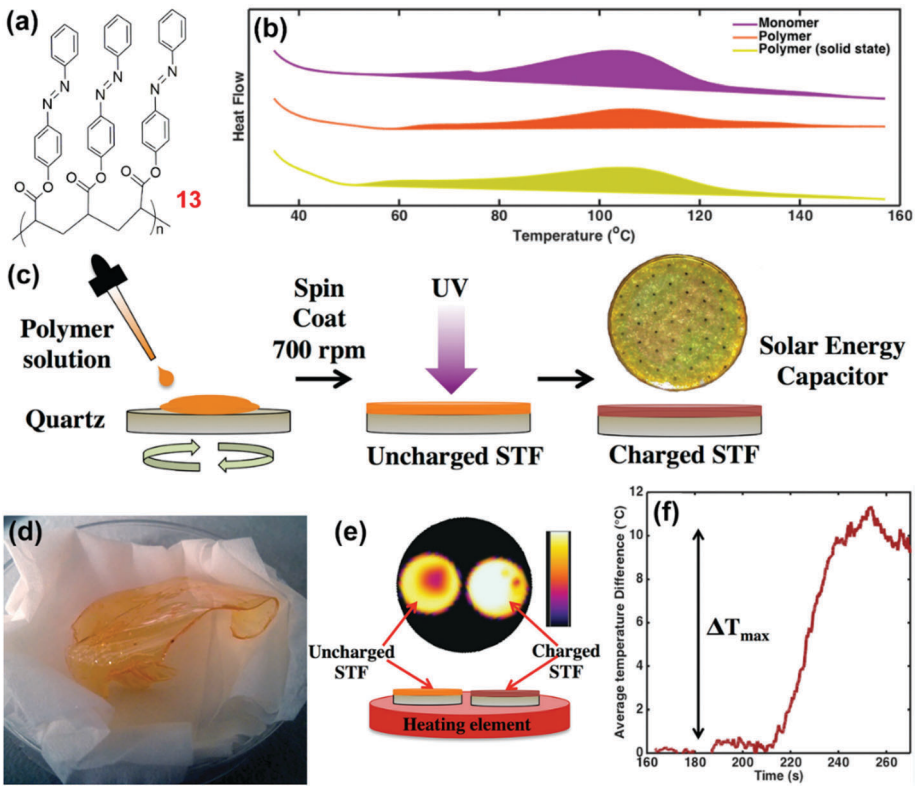

Fig. 13 (a) Chemical structure of Azo-polymers. (b) DSC curves of charged monomers and polymers. (c) Schematic of spin-coating a polymer solution in toluene on a transparent quartz substrate. The charging process is accomplished under UV irradiation using a lamp of wavelength 365 nm. (d) Photograph of a large-area freestanding polymer film prepared by the cross-linking approach. (e) Heat release in STF polymer films: top-view is IR heat map of charged and uncharged STFs; the color bar indicates the relative heat magnitude. Bottom-view is the illustration of the experimental setup. (f) Average temperature differences between the two STFs. A temperature difference of at least 10 °C is observed between the two STFs because of heat release. Reprinted with permission from ref. 148. Copyright 2016 Wiley-VCH.

experimental setup that employed a heating stage to trigger the *cis*-to-*trans* thermal isomerization (Fig. 13e). In the meantime, an infrared camera was applied to measure the spatial temperature profile. A dramatic temperature spike of 10 °C average temperature variation between the charged and uncharged STFs can be observed in Fig. 13f. Furthermore, the temperature difference caused by heat release in tens of seconds plays a vital role in certain rapid heat-release applications. However, on the other hand, the introduction of superfluous groups and polymers results in limited heat release and heat propagation.

Previous research showed that different solvent processing could change the physical properties of polymers to tune the ED, heat-release shape, and activation energy of *cis*-to-*trans* isomerization of STF materials. Most recently, Venkataraman *et al.* studied the crucial role of processing solvents and thin film structures in achieving higher EDs. They developed azobenzene-based syndiotactic-rich poly(methacrylate) polymers (Fig. 14a, **14a–c**) and achieved a high-ED STF with a maximum value of 698 J g^{-1} (correspond to 194 W h kg^{-1}).[151] In this study, dichloromethane (DCM) and tetrahydrofuran (THF) were chosen to understand the role of polymer–solvent interactions and optimal structures in achieving high EDs based on the fact that both THF and DCM are excellent solvents for polymer **14c**. Polymer chains extend in a good solvent, which provides an environment for high polymer–polymer interactions. Moreover, THF and DCM have low boiling points, which allows their removal at low temperatures without adversely affecting the *cis–trans* isomer ratio. As shown in Fig. 14b, the DSC curves of samples dried from DCM display a lower ED than that of the samples obtained from THF. To be specific, the samples dried from DCM had an average ED of 110 J g^{-1} (30.6 W h kg^{-1}), while the sample obtained from THF exhibited an average ED of 510 J g^{-1} (142 W h kg^{-1}). Moreover, they mixed THF with DCM in various ratios and measured the full width at half maximum (FWHM) and the ED of polymer **14c**. They found that the FWHM increased and the ED decreased with increasing DCM ratio (Fig. 14c). The main reason is that DCM preferentially interacts with the polymer backbone but does not solvate the dipole formed in the charged *cis*-Azo, leading to aggregation in solution. This aggregation further leads to a compact inter-polymer packing, a more disorderly alignment of dipoles, and insufficient volume between the polymer backbones for π–π stacking between the pendant *cis*-Azo after isomerization. Finally, these factors give rise to a solid active layer that lacks cooperative isomerization, thereby resulting in lower EDs. It is inferred that the processing solvent should sufficiently solvate the dipole formed in the charged state to reduce aggregation in solution and lead to optimal structures that allows efficient π–π stacking to achieve a high ED.

Despite the advances in the integration of polymer-templated azobenzene thin films into certain solid-state devices, many of such materials need to be obtained in solution and a formidable difficulty often exists in their transition to the solid state in an efficient manner. Electrodeposition is a fast, conventional, and reliable synthetic technology, which has been widely applied for the preparation of polymer on a conducting surface. Electrodeposition on conducting substrates employs solutions with a low monomer concentration and allows the utilization of various form factors, to give maximum product yield. Based on this consideration, Grossman and co-workers designed novel polymer-templated azobenzene STFs that could be readily obtained by electrodepositing azobenzene and a carboxylic acid-based monomer on different sorts of substrates through copolymerization (Fig. 15a). The substrates could be either flat or structured, depending on the applications (Fig. 15b and c).[152]

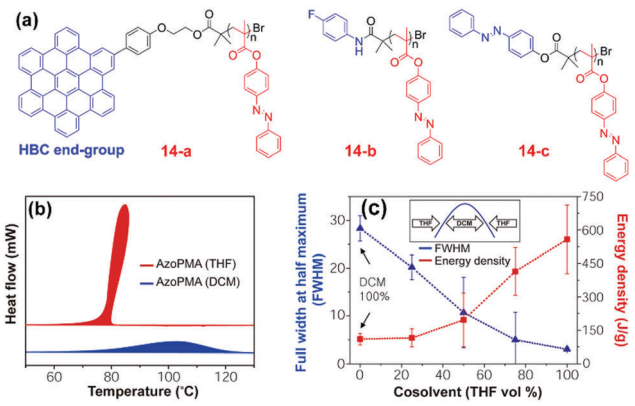

Fig. 14 (a) Chemical structures of Azo polymers with different end-groups. (b) DSC curves of a *cis*-Azo sample (**14c**) dried from either THF or DCM. (c) Diagram of FWHM and energy density of Azo-polymer (**14c**) based on different co-solvent ratios of THF and DCM. Reprinted with permission from ref. 151. Copyright 2017 Springer Nature.

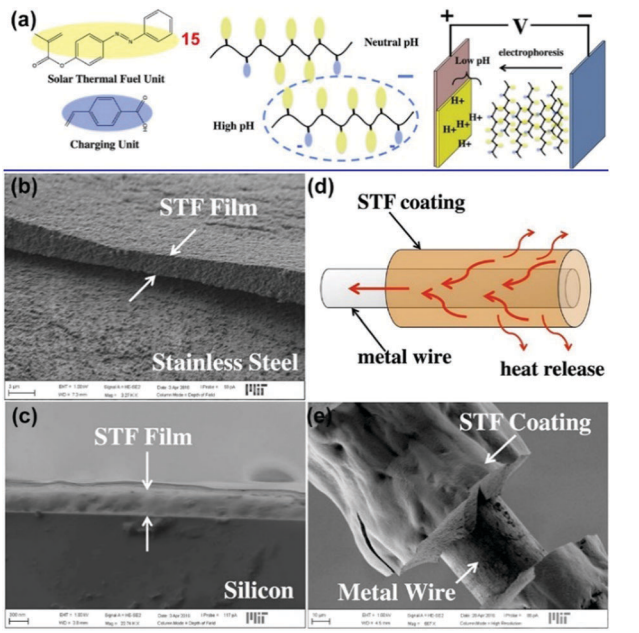

Fig. 15 (a) Chemical structure of Azo-polymers and concept of the electrodeposition scheme. Cross-sectional SEM images of the electrodeposited polymer films on (b) stainless steel and (c) silicon substrates. (d) Concept of a STF fiber in which solar energy is stored in the STF coating, released as heat into the metal wire, and transported along the wire to desired locations. (e) Proof-of-concept for an Azo-STF fiber. Reprinted with permission from ref. 152. Copyright 2016 American Chemical Society.

Furthermore, this approach allowed the tuning of thickness *via* controlled deposition conditions, generating highly uniform films over a large area. Based on the systematic study of the polymer films, they proposed a potential application in the form of STF fibers, where the azobenzene-containing polymer is coated on a thin metal wire surface and integrated into fabrics (Fig. 15d). Consequently, the low-thermal conductivity Azo-STFs combined with high-thermal-conductivity metals would efficiently transfer heat to other parts of the fabric or device. Finally, the authors fabricated an Azo-STF coated wire, as shown in Fig. 15e. The solar energy is stored in the Azo-STFs under UV irradiation. The stored energy would be released as heat *via* *cis*-to-*trans* isomerization and could be directionally transported along the wire to desired locations. This study proved that electrodeposition is an effective way of incorporating Azo-STFs into novel solid-state applications. Moreover, additional functional groups or molecules could be easily introduced into the polymer-templated Azo-STF material *via* copolymerization without any major compromise on the ED of the STFs. Nonetheless, there is one problem that should be noted. At higher thicknesses, the film may exhibit cracks and deformities due to the high degree of shrinkage during the drying process. Thus, the future research on such fiber STFs may be directed toward the design of high-molecular weight azobenzene-containing polymers or the addition of binders while minimally affecting the ED of the STFs.

3.3.2 Azo-STFs based on crystal-to-liquid phase transition. Although much progress has been made in improving and controlling the properties of STFs in the solid state, as shown in the previous studies by using polymer templates and molecular engineering, little work has been done in controlling the specific packing to increase the ED of Azo-STFs. Since the polymer systems showed a decrease in stored ED, a better understanding of the close packing of azobenzene molecules may help improve the storage properties in solid-state STFs.

Recently, Morikawa's research group provided a new perspective that the collective change in *cis*-to-*trans* isomerization of Azo-STF materials could be observed as a macroscopic crystal-to-liquid phase transition. The crystal-to-liquid phase transition could impart extra energy to the azobenzene in the exothermic process.[153] In this study, Morikawa *et al.* developed ionic crystals (ICs) of azobenzene derivatives, which consist of spacers with various methylene lengths (m) and alkyl tails (n), an oligo(ethylene oxide)-based ammonium group, and a counter ion (X) (Fig. 16a, **16**). The polymer-templated azobenzene ICs showed a phase transition from IC to ionic liquid (IL) upon UV irradiation. Reversibly, the *cis*-azobenzene ILs crystallized to *trans*-azobenzene ICs by visible-light irradiation. This conversion is accompanied by a total exothermic enthalpy of 97.1 kJ mol^{-1} (128 J g^{-1} or 36 W h kg^{-1}), which is more than twice the energy stored in pure *cis*-Azo.

Fig. 16b shows the X-ray diffraction (XRD) profiles and polarizing optical microscopy (POM) images of the 1(6,4)-Br azobenzene derivative subjected to different treatments. The POM image of the as-prepared film exhibits a birefringence phenomenon, which is consistent with the crystalline lamellar

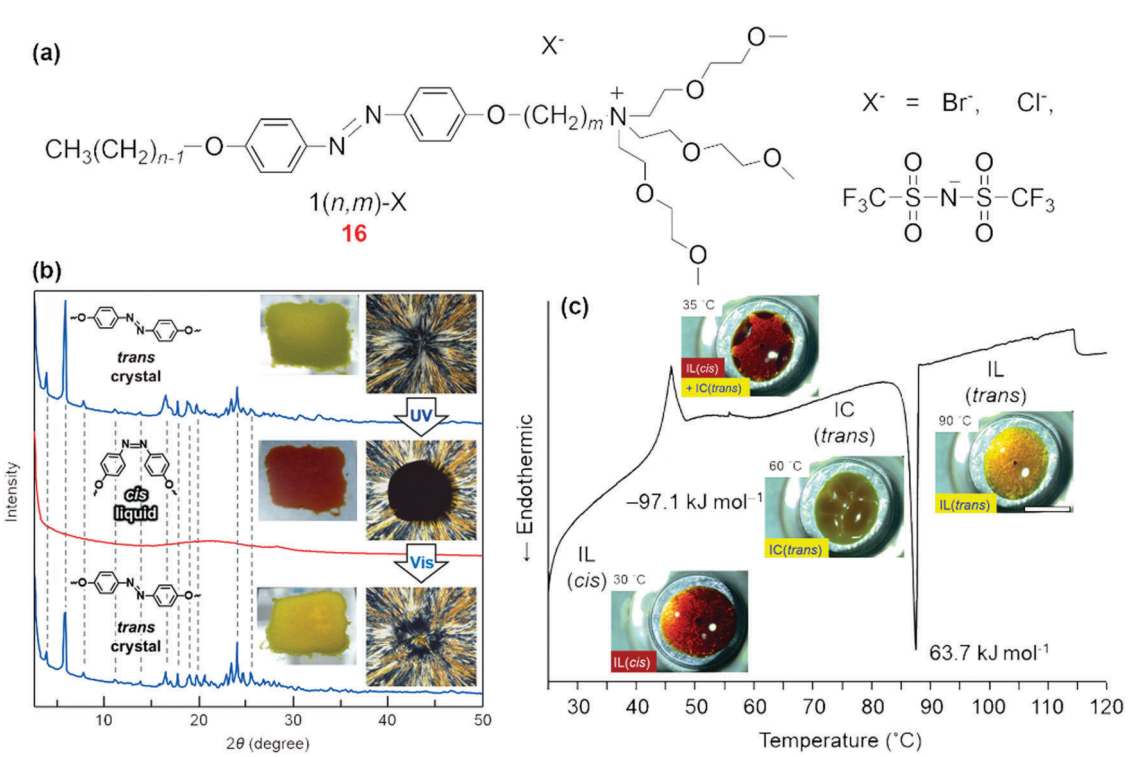

Fig. 16 (a) Chemical structure of cationic azobenzene derivatives 1(n,m)-X. (b) XRD profiles of 1(6,4)-Br prepared on a silicon wafer: from top to bottom are the as-prepared film, UV-light-irradiated film, and visible-light-irradiated film, respectively. Picture of each sample is shown as an inset. (c) DSC curves of *cis*-1(6,4)-Br. Photographs of corresponding states are shown as insets. Reprinted with permission from ref. 153. Copyright 2015 Wiley-VCH.

structure as shown in the XRD graph. Under UV irradiation, the yellow crystal sample melted into a red liquid phase accompanied by a conformational change of azobenzene from *trans* to *cis*. It should be noted that the irradiated part appeared dark under the POM with crossed polarizers. These measurement results indicated that the photoisomerization of *trans*-1(6,4)-Br azobenzene caused its liquefaction into an isotropic IL. Then, the reversible crystallization of the *cis*-azobenzene IL occurred upon visible-light irradiation, and the XRD profile showed the characteristic peak of *trans*-azobenzene. These observations clearly demonstrated reversible photocrystallization and photoliquefaction of the 1(6,4)-Br azobenzene derivative. Fig. 16c shows the DSC curves of *cis*-azobenzene IL. Unlike in previous studies, two coexisting exothermic peaks could be observed in the temperature range of 34 to 65 °C. The broad peak was ascribed to thermal *cis*-to-*trans* isomerization of azobenzene, while the sharp exothermic peak around 46 °C was attributed to the enthalpy of phase transition of *cis*-azobenzene IL to *trans*-azobenzene IC. As the heating continued, a sharp endothermic peak appeared at 87 °C, which is associated with the melting of *trans*-azobenzene ICs. Thus, the photoinduced *trans*-IC to *cis*-IL phase-transition Azo-STF technology pushes the limit of current energy storage capacity.

Similarly, Grossman's group took the same view and reported a series of azobenzene-functionalized symmetric diacetylenes, as shown in Fig. 17 (**17a–h**).[154] Diacetylenes can be facilely functionalized and tend to self-assembly into crystalline-like packing because of strong intermolecular interactions. Under UV irradiation, the diacetylene monomers rapidly photopolymerize to polydiacetylenes with azo-containing side chains on the rigid conjugated backbones. This structure is analogous to a rigid template decorated with closely packed photoswitching units (Fig. 17b). Fig. 17c shows a new energy diagram of STF materials that undergo phase change by isomerization of azobenzene. A high ED was obtained for the resulting materials, which could store solar energy of 176 kJ mol^{-1} (243 J g^{-1} or 67.5 W h kg^{-1}) for compound **17d** and 173 kJ mol^{-1} (239 J g^{-1} or 66 W h kg^{-1}) for polymer **17d**. According to the understanding gained from the systematic research of the series of molecules in this work, the authors believed that the molecules with high crystallization energies were very suitable for the design of high-ED Azo-STFs. They suggested the following design principle for high-ED

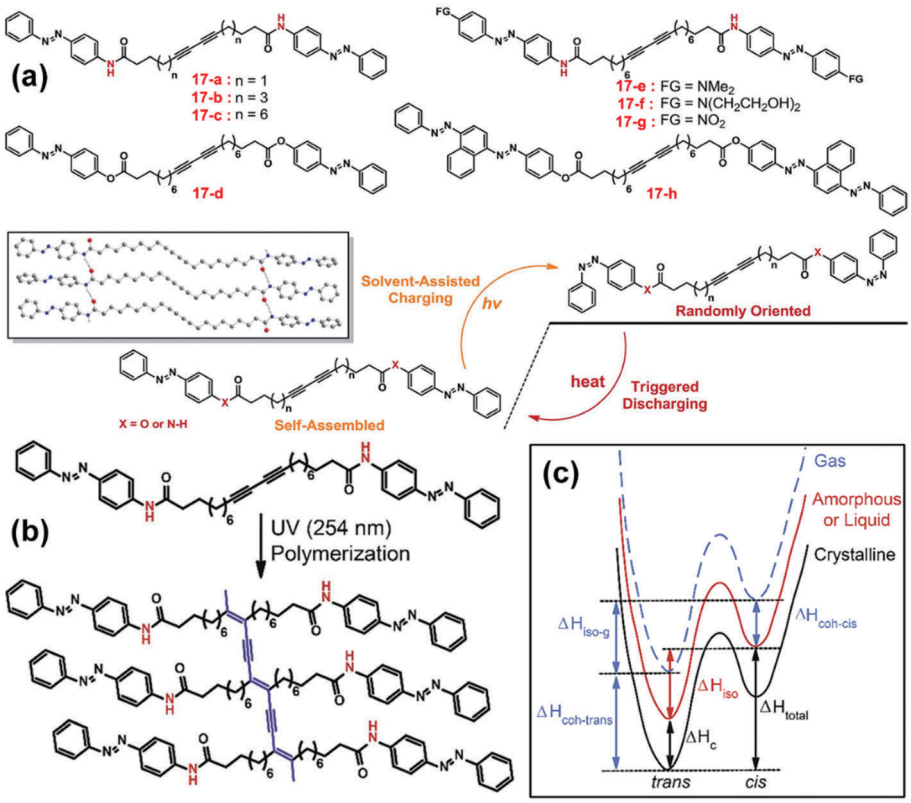

Fig. 17 (a) Chemical structures of Azo-functionalized diacetylenes with diverse alkyl chain lengths, terminal functional groups, H-bonding units, and an extended p-system along with a schematic of photoisomerization and reverse isomerization of compounds **17a–d**. The inset shows a crystal structure of azobenzene derivative (**17c**). (b) Scheme of photopolymerization of monomers and the structure of the resulting polymer. (c) Energy diagram of azobenzene derivatives in different phases (gas, amorphous or liquid, and crystalline). ΔH_{iso} is the isomerization energy of azobenzene derivatives in the liquid state or amorphous solid, and ΔH_c is the crystallization energy of the *trans* form of azobenzene derivatives from the liquid state or amorphous solid to crystalline solid. $\Delta H_{coh\text{-}trans}$ is the cohesive enthalpy of *trans*-azobenzene derivatives from the gas state to the crystalline solid, and $\Delta H_{coh\text{-}cis}$ is that of *cis*-azobenzene derivatives from the gas state to the amorphous solid or liquid state. $\Delta H_{iso\text{-}g}$ is the thermal isomerization enthalpy between *trans* and *cis* isomers in the gas phase. ΔH_{total} is the heat released from the materials after UV irradiation, which can be expressed as the sum of ΔH_{iso} and ΔH_c. Reprinted with permission from ref. 154. Copyright 2016 Royal Society of Chemistry.

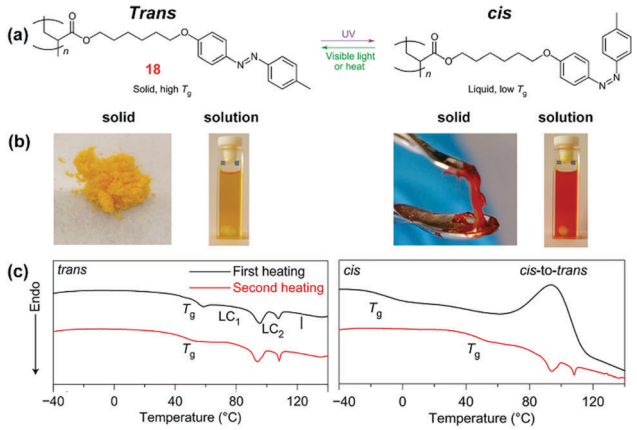

Fig. 18 Chemical structure (a), photographs (b), and DSC curves (c) of Azo-polymers, which are polyacrylates with a flexible spacer and an azobenzene group on the polymer side chain. The *trans*-Azo polymer is solid but the *cis*-Azo polymer is liquid. Reprinted with permission from ref. 155. Copyright 2017 Springer Nature.

Azo-STFs: the *trans* form of azobenzene should self-assemble to form a crystalline structure and the *cis* isomers should become liquid through the photoisomerization process.

Most recently, Wu *et al.* demonstrated that the glass transition temperature (T_g) of Azo-based polymers (**18**) could be tuned through light irradiation, thus inducing reversible solid-to-liquid transitions of the polymers (Fig. 18a).[155] The *trans*-Azo-polymers are solids with T_g above room temperature, whereas the *cis*-Azo-polymers are liquids with T_g below room temperature (Fig. 18b). The DSC curve confirmed that the photoinduced solid-to-liquid transition of the polymer was due to its photoswitchable T_g. Although the photo-energy storage properties of these Azo-polymers are not the subject of research in this work, they may provide a new perspective in the study of solar thermal storage technology.

3.3.3 Full-spectrum Azo-STFs. In most Azo-STFs, UV light is often used to accomplish *trans–cis* isomerization. However, sunlight contains only about 5% UV light, which severely limits the absorption efficiency of Azo-STFs. Therefore, it is of paramount importance to develop an Azo-STF that could efficiently work across the full solar spectrum. Many studies demonstrated that the introduction of substituents to azobenzene can change the absorption bands.[156–158] Based on previous studies,[155,159] Wu *et al.* proposed an Azo-STF device that can efficiently store both UV and visible light upon full solar irradiation (Fig. 19a and b).[80] As can been seen in Fig. 19c,

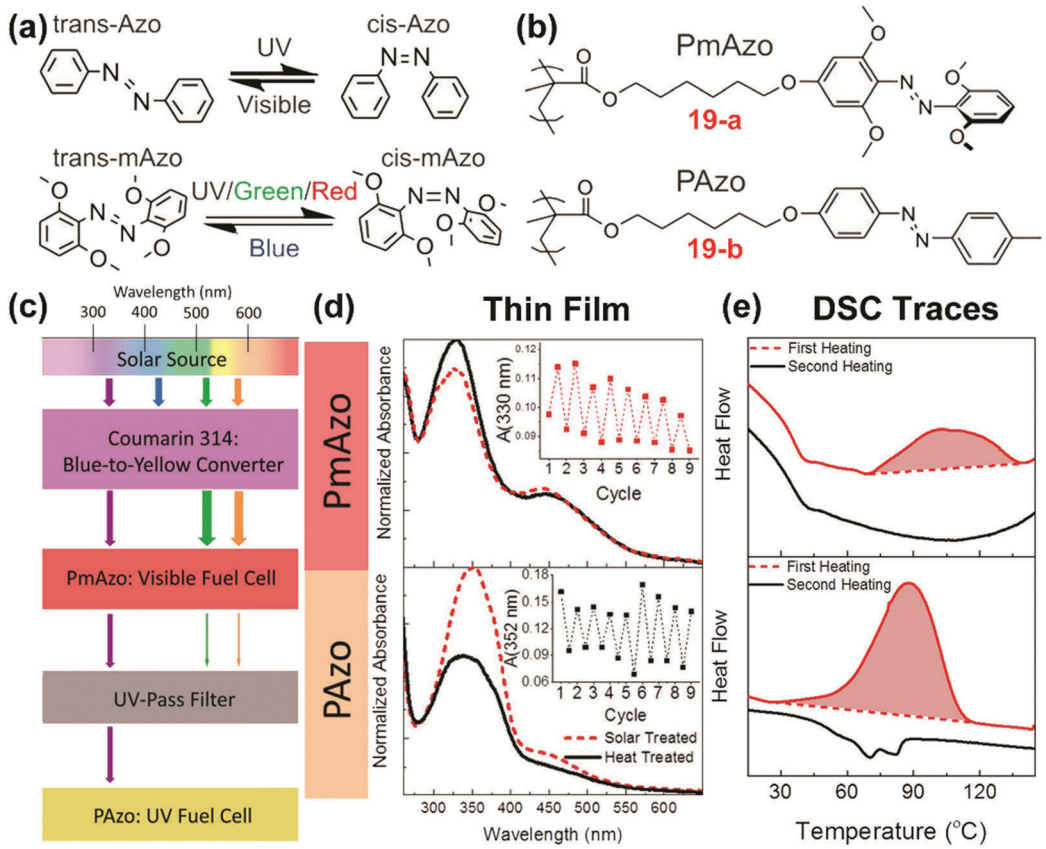

Fig. 19 (a) Reversible photoisomerization of Azo and mAzo chromophores. (b) Chemical structures of UV-responsive polymers (PAzo) and visible-light-responsive polymers (PmAzo). (c) Schematic illustration of four-layered solar thermal cell. (d) UV-vis spectra of PAzo and PmAzo films upon 1 h solar irradiation followed by 2.5 h heating in a vacuum oven at 90 °C. The insets show the tracking absorbance of the π*–π band of PAzo and PmAzo with different cycles. (e) DSC curves of PAzo (365 nm, 2 mW cm^{-2}, 20 min) and PmAzo (530 nm, 4 mW cm^{-2}, 40 min). Reprinted with permission from ref. 80. Copyright 2017 Wiley-VCH.

the device consists of PmAzo (**19a**), PAzo (**19b**), Coumarin 314, and a UV-pass filter. In such a four-layered hybrid device, two active layers of PAzo and PmAzo were used to store solar energy through the photoisomerization of the Azo group on the polymer side chains, while the other two filtering layers were used to modify the effective incident spectrum.

In the experiment, the spin-coated films of PAzo ($\approx$35 nm) and PmAzo ($\approx$20 nm) were integrated into the STF device with all solid layers. As shown in Fig. 19d, the UV-vis spectra indicate the expected increase in the n–π* transition and decrease in the π–π* transition upon UV irradiation of amorphous polymer PmAzo, due to the *trans*-to-*cis* isomerization. Interestingly, the *trans*-to-*cis* photoisomerization of PAzo led to an increase in the π–π* transition intensity, which might result from the characteristic photochemical phase transition of liquid crystalline azopolymers PAzo. As is known, the *trans*-Azo groups in liquid crystalline azopolymers preferably orient perpendicular to the substrate.[160] Upon UV irradiation, the azopolymer changed from a ''frozen'' liquid crystalline state to an amorphous state. On one hand, the π–π* transition band decreased due to the partial photoisomerization of *trans*-isomers to *cis*-isomers. On the other hand, the π–π* transition band increased because a more random orientation of azobenzene chromophores was formed by shifting away from the perpendicular orientation. From the DSC measurements shown in Fig. 19e, the *cis–trans* enthalpy difference was found to be 12.2 kJ mol^{-1} (14.4 J g^{-1} or 4.4 W h kg^{-1}) for PmAzo and 54.8 kJ mol^{-1} (125.2 J g^{-1} or 34.8 W h kg^{-1}) for PAzo. The experimental results indicated that *cis*-Azo conversion of 60–70% upon monochromatic irradiation was achieved through the selective blocking of light that could induce *cis–trans* back-isomerization. It is expected that a remarkable enhancement in the solar efficiency could be achieved by the rational device design and improved spectral overlap.

In summary, polymer-templated Azo-STFs offer the possibility of tuning the monomer structure and polymer backbone to enhance the solar energy storage capacity, light absorption efficiency, and photoisomerization degree, and allow the collection of photons over a wide range of the solar spectrum. Table 3 summarizes the ED, half-life, and *cis* $\leftrightarrow$ *trans* state of polymer-templated azobenzene STF materials. Compared to carbon-templated Azo-STFs, polymer-templated Azo-STFs have relatively lower EDs and half-lives. Moreover, Azo-based polymers can be easily integrated into existing heating equipment and may have tremendous potential for the development of novel energy storage and heat release applications because of their solid state, controllable liquid-to-crystal transition for extra energy, and triggerabilty for heat release. This is the most important advantage of polymer-templated Azo-STF materials.

4. Emerging strategies toward efficient solar thermal fuels

The Azo-STF technology has proven to be an efficient, very promising, and versatile tool for solar-thermal conversion and storage solutions. STF materials such as pure azobenzene derivatives, nanocarbon-templated azobenzene hybrids, and polymer-templated azobenzene have shown their potential for favorable solar spectrum matching, stimulated heat release, and robust, multicycle systems. In addition, these systems are being re-explored using modern computational approaches which bring new opportunities for future molecular design. Although great steps have been taken with regard to Azo-STF materials, the development is still in a very preliminary stage. This fast-growing research field is still restricted by their low ED, short half-life, irreversible degradation, and small overlap with the solar spectrum. However, challenges are also opportunities. In this section, we discuss the emerging molecular design of Azo-STFs with high-energy storage capacities as a strategy to overcome the aforementioned limitations.

4.1 Solar thermal fuels with high energy density

The maximum ED of Azo-STFs is typically determined by both the standard free energy of the *cis*-to-*trans* isomerization reaction ($\Delta H_{\text{storage}}$) and the fraction of the *cis*-isomer in the photostationary state. Thus, the strategy for increasing the ED is mainly focused on these two aspects. Below, we discuss several strategies that can increase the ED of Azo-STFs.

4.1.1 Azo-STFs based on phase-change systems. The phase change of a material is closely related to intermolecular interactions, such as van der Waals forces, dipolar interactions, and hydrogen bonding. In addition, the difference between the *trans* and *cis* states of azobenzene can cause a change in the geometry, length, planarity, and dipole moment. The collective

Table 3 Parameters related to polymer-templated Azo-STFs

	Energy density					
Polymer-templated Azo-STFs	(kJ mol^{-1})	(J g^{-1})	(W h kg^{-1})	$\tau_{1/2}$	State	Ref.
13	[a]	104	29	55 h	Solid	148
14-a	[a]	373–469	103–169	[a]	Powder	151
14-b	[a]	337–551	94–153	[a]	Powder	151
14-c	[a]	395–625 (698 is the highest)	110–174	[a]	Powder	151
15	[a]	85–95	24–26	75 h	Solid	152
16	97	128	36	[a]	Liquid $\leftrightarrow$ crystals	153
17	173 (the highest)	239	66	98 h (monomer)	Liquid $\leftrightarrow$ crystals	154
19a	12	14	4	16	Liquid	80
19b	55	125	35	12	Liquid	80

[a] No data were found in the references.

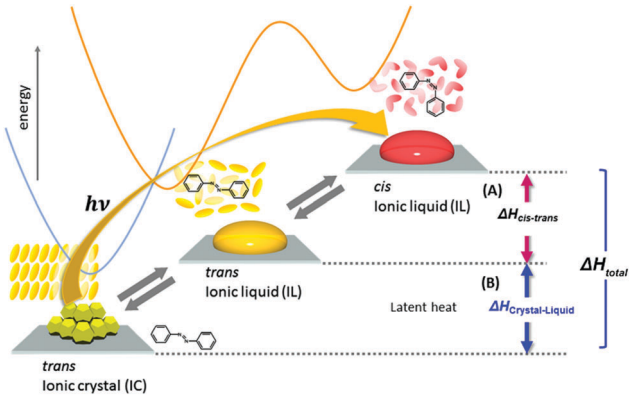

Fig. 20 Schematic diagram of a photoinduced crystal-to-liquid phase transition and its associated enthalpy change. Reprinted with permission from ref. 39. Copyright 2016 American Chemical Society.

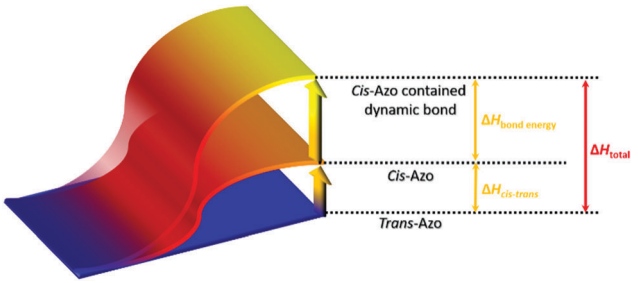

Fig. 21 Schematic illustration of a STF system that combines azobenzene and dynamic covalent bonds.

change in these intermolecular interactions in such materials eventually causes the macroscopic solid–liquid phase transition. The solid–liquid phase transition can bring extra energy to the azobenzene in the exothermic process. Therefore, the *trans* and *cis* states affect the material phase, giving leverage to the storage ED (see in Fig. 20). Furthermore, phase transitions of matter are generally induced by heat. In contrast, azobenzene undergoes photoinduced transition between solid and liquid phases at a constant temperature. Thus, the concept of utilizing the structural difference between the *trans* and *cis* states of azobenzene to influence the phase change properties and increase the ED of Azo-STFs is interesting and promising.

Although the previous works mentioned in Section 3 have already demonstrated that the solid–liquid phase change characteristic of azobenzene derivatives could impart extra energy to the STFs,[153–155] the development is still in a nascent stage. Many basic challenges and critical issues remain to be resolved. The phase transition temperature of azobenzene derivatives is generally above 80 °C, which inhibits its practical applications. If we can lower the phase transition temperature and design an azobenzene derivative, in which the *trans* form of azobenzene is solid but the *cis* form is liquid at a relatively lower temperature (or even at room temperature), we can greatly contribute to the existing PCMs. Based on these considerations, we believe that the next research direction of phase-change Azo-STFs would involve the exploitation of chemistry associated with the design and development of molecular systems. Luckily, the ability of a wide variety of azobenzene derivatives to undergo photoinduced reversible phase changes has been recognized for almost two decades.[161–166] Plenty of macrocyclic and linearly structured azobenzene derivatives have already been discovered, which can help us explore the potential of phase-change Azo-STF systems.

4.1.2 Azo-STFs based on dynamic covalent bond systems. Dynamic covalent bonds, *i.e.*, reversible covalent bonds, can form under one condition and cleave in another under diverse external stimuli such as light, temperature, pH, oxidation, and reduction.[167,168] Based on the bond connections, dynamic covalent bonds can be categorized into C–N bonds, C–C bonds, C–O bonds, C–S bonds, S–S bonds, and B–O bonds (as summarized in Table 1 of ref. 138 and 169 in addition to Se–Se and Se–N bonds developed by Zhang and Xu recently).[170–174] Dynamic covalent bonds and azobenzene share three common aspects: (i) they transform from one stable state to another under external stimuli, (ii) they involve the cleavage and reformation of chemical bonds (rotation or inversion of N=N for azobenzene and formation and cleavage of covalent bonds for dynamic covalent bonds) resulting in energy change, and (iii) they exhibit superior reversibility and cyclability. These similarities provide the opportunity to introduce dynamic covalent bonds into Azo-STF materials.[175,176] Fig. 21 shows the basic mechanism of increasing the ED of a STF system by combining azobenzene with dynamic covalent bonds. It can be foreseeable that the combination of dynamic covalent bonds and Azo-STFs will greatly increase the ED of existing Azo-STFs and may endow them with other surprising properties such as changeability and tunability. According to the Pauling equation, the bond energy of a disulfide bond is estimated as 240 kJ mol^{-1},[177] which is more than four times that of pristine azobenzene. If we can combine the dynamic nature of disulfide bonds and the conformation switching property of azobenzene under UV irradiation through proper molecular design, we will probably achieve an ultrahigh-ED Azo-STF material. The design and synthesis of Azo-polymers based on disulfide metathesis are currently underway in our research group.

4.1.3 Fraction of *cis*-Azo. Another strategy for increasing the ED of Azo-STFs is to increase the fraction of *cis*-Azo in the photostationary state. The photostationary state of azobenzene contains not only the *cis*-isomer, but also the *trans*-isomer. It is easy to understand that the higher the quantum yield, the greater will be the *cis*-Azo fraction in the photostationary state. Thus, we should have the ability to control the degree and rate of photoisomerization and back-isomerization. Many factors can influence the quantum yield and photoisomerization mechanism, including the state of azobenzene,[178] thermal isomerization of *cis*-Azo,[109,179] irradiation wavelength,[118,180,181] solvent properties,[182–184] substituents on the phenyl rings of azobenzene,[108,185–187] temperature,[183,188–190] energy gap between the π–π* and n–π* states,[111,127] and pressure.[191–193]

There is a paucity of literature on the quantum yield of photoisomerization measured in the solid state.[178,194–196] This is mainly because photoisomerization is not uniform across the entire film thickness, and the degree of photoisomerization

largely depends on the local light intensity. As a result, the pattern describing the *trans*-to-*cis* conversion in the solid state exhibited a more complex problem than in solution. In fact, the experimental procedure is more intractable than in solution because of the spatial distribution of light intensity.[197] Therefore, much effort has been focused on factors affecting the isomerization of azobenzene molecules in the liquid state.

Polarity and viscosity can influence the isomerization mechanism. Burdette *et al.*[81] summarized the polarity and viscosity of solvents that affect the quantum yield of isomerization of azobenzene. Non-viscous polar solvents were found to favor rotation, while inversion was preferred in viscous non-polar solvents. Serra *et al.*[198] investigated the kinetics of photoisomerization and thermal isomerization of an azobenzene-containing acrylate molecule in solvents with different polarities (chloroform, toluene, and *N*-methylpyrrolidone) mixed with different contents of polystyrene to increase the viscosity. The results indicated that the photoisomerization constant was slightly correlated with solvent polarity, whereas the thermal isomerization constant was largely dependent on solvent viscosity and polarity.

Several studies[188,189] have shown that the quantum yield of photoisomerization could not be significantly affected by temperature; however, the quantum yield of back-isomerization decreases significantly with an increase in temperature. Yoshii *et al.*[190] investigated the photoisomerization of azobenzene at low temperatures, which indicated that the *trans*-to-*cis* isomerization cannot be frozen out completely even at 4 K. Besides, the thermal back-conversion should be considered when analyzing the photoisomerization quantum yield. Many theoretical and experimental studies[111,199,200] have indicated that rotation and inversion might be the pathways for thermal isomerization. Hecht *et al.*[201] carried out an extensive theoretical study on the *cis*-to-*trans* isomerization of substituted azobenzenes (type, number, and substitution position) in a polarizable environment and gas phase. In the case of a single substituent, the linear transition state could be efficiently stabilized with EWGs at *ortho* and *para* positions. In the case of two or three substituents, substitution on one side of the benzene ring has an accumulative effect on kinetics and activation energies, whereas, for the substitution on both the phenyl rings, no simple additivity rule was discovered. In the case of 4-donor–4′-acceptor-substituted azobenzene, the isomerization mechanism relied on the solvent, and inversion was preferred in nonpolar solvents while rotation in polar environments. Furthermore, the 4-donor–4′-acceptor-substituted azobenzene showed a lower energy of the transition state and faster rate of thermal isomerization. With increasing solvent polarity, the activation energy decreased, whereas the thermal back-isomerization rate increased.[202,203] Moreover, hydrogen-bonding solvents were found to accelerate the *cis*-to-*trans* isomerization compared to aprotic solvents with a similar polarity.[204,205]

Most importantly, the substituents of azobenzene could dramatically change the isomerization of azobenzene by steric and electronic effects.[206] The photoisomerization of EDG-functionalized azobenzene has been well studied using the time-resolved spectroscopic methods.[117,184] It shows a rapid photoisomerization that leads to the lowest lying π–π* transition. Roitberg *et al.*[108] studied a series of azobenzene derivatives to determine the substituent effects on the isomerization pathways by using *ab initio* methods. They have found that appending EDGs to the phenyl rings of azobenzene could increase the ground-state inversion barrier height, resulting in a more difficult back-reversion. In contrast, EWGs were found to lower the same barrier. *p*-Nitroazobenzene as a typical EWG-functionalized azobenzene has been investigated by resonance Raman spectroscopy.[207] It was observed that within 20 fs of photoexcitation of *p*-nitroazobenzene, the stretching vibrations of N=N and C–N bonds undergo great changes and the unsubstituted phenyl ring and the nitro stretching vibrations are also significantly distorted. Furthermore, for di-substituted azobenzenes, such as *p*-diaminoazobenzene, the symmetric di-substitution could influence the S_0 isomerization surface.[206] In 4-donor–4′-acceptor-substituted azobenzene, photoisomerization is dominated by rotation. The character of its excited states could be strongly altered through the push–pull substitution of azobenzene.[208,209]

In the above discussion, the factors affecting the isomerization reaction of azobenzene photoswitches are presented with the aim of tuning the switching process. Upon light absorption, azobenzene will go through various transformations, which are associated with photoisomerization and other energy dissipation processes. The degree of photoisomerization and the rate of thermal isomerization of azobenzene depend on factors such as the polarity and viscidity of the solvent, temperature, free volume, thermal isomerization, and substituents. Thus, when designing high-ED Azo-STF materials, we should consider these factors as much as possible so that the maximum fraction of *cis*-Azo can be achieved in the photostationary state.

4.2 Solar thermal fuels with long-term thermal storage

It is well known that the half-life of azobenzene is strongly dependent on the energy barrier of *cis*-to-*trans* reversion. In most azobenzene derivatives, $\tau_{1/2}$ is approximately from minutes to hours or a couple of days. A short-lived *cis*-Azo implies that strong light irradiation is required to maintain a large fraction of the *cis*-isomer in the photostationary state; this will further shorten the half-life owing to the thermal radiation of the intense light source. This limitation is undesirable for Azo-STFs. Thus, the utility of an Azo-STF is contingent on not only its energy density, but also its half-life. It is a very challenging task to increase the half-life of azobenzene while retaining a high ED for Azo-STFs. In the past few years, scientists have developed a couple of newly designed azobenzene photoswitches that may provide the optimum solution to this problem.

2,2′-Ethylene-bridged azobenzene (br-Azo) refers to a class of azobenzene that bridges an ethylene linker at the two *ortho*-positions of azobenzene.[156,210] Such a short bridge severely strains and distorts the *trans*-isomer, which leads to the existence of the *trans* form of br-Azo in two conformations: chair and twisted forms. On the other hand, the *cis*-isomer has a boat configuration, which is more stable than the *trans*-isomer (Fig. 22a).[211] Interestingly, introducing an ethylene bridge leads

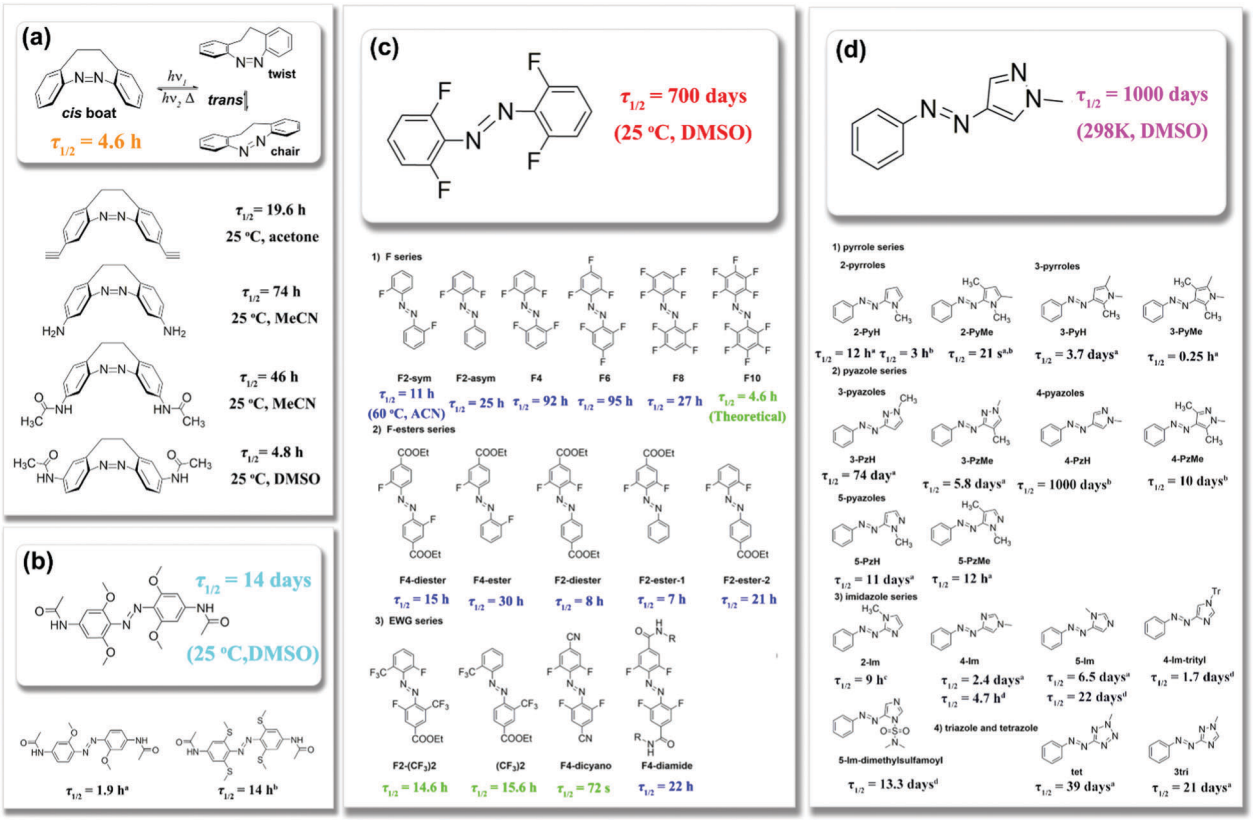

Fig. 22 Chemical structures of long half-life azobenzenes: (a) bridged Azo, (b) tetra-*ortho*-methoxy Azo, (c) *ortho*-fluoroazobenzenes, and (d) azoheteroarene.

to two odd consequences: (i) the *cis* form of azobenzene becomes thermodynamically more stable (the half-life was found to be 4.5 h at 28.5 °C), and (ii) the *trans* and *cis* isomers exhibit very distinct n–π* absorption bands. It turned out that the br-Azo exhibits much superior photophysical properties (such as quantum yields and switching efficiencies) compared to the parent azobenzene and other commonly used azobenzene derivatives.[212–216] This makes them ideal candidates for solar harvesting and storage applications. Furthermore, the photoisomerization of br-Azo was studied by nonadiabatic *ab initio* and density-functional-based molecular dynamics simulation.[217–222] It was found that the bridging feature in the *trans* form of br-Azo does not hinder rotation around the N=N bond but renders the twisting of the two phenyl rings around the C–N bonds much slower. A number of br-Azo derivatives have been synthesized in the past decade, some of which have relatively long half-lives (Fig. 22a).[211,220,223] We hope that researchers will get some inspiration from these br-Azo compounds.

The tetra-*ortho*-substituted azobenzene derivatives were found to be highly promising such as the *ortho*-fluorinated compounds reported by Hecht and Bleger,[224,225] and the *ortho*-methoxy analogues reported by Woolley *et al.*[158] Fig. 22b and c summarize the half-lives of the tetra-*ortho*-substituted azobenzene derivatives. For tetra-*ortho*-methoxy azobenzene, the substituents at the *ortho*-position could distort the typically planar structure of the *trans*-isomers. This distortion is caused by the repulsive interactions between the O and N lone pair electrons, which inevitably destabilizes the energy of the π and π* molecular orbitals. This will increase the energy level of all the orbitals and eventually result in a longer half-life (about 14 days). On the other hand, the F atom as an EWG would lower the electron density in the nearby N=N bond, resulting in a decrease in the n-orbital energy and stabilization of the *cis* form of F-Azo, thereby exhibiting an unprecedented long half-life ($\tau_{1/2}$ = 700 days at 25 °C). Thus, the tetra-*ortho*-substituted azobenzenes proved great candidates for long-term STFs.

Fuchter and co-workers recently reported an alternative approach, wherein one of the aryl rings from the conventional azobenzene family was displaced by a five-membered heteroaromatic ring, *i.e.*, azoheteroarenes (Fig. 22d).[226–229] Although the new class of azobenzene photoswitches is relatively understudied, they have significant potential (excellent photoswitching property and long *cis*-isomer half-life) as compared to other more common azobenzene counterparts. The computational and experimental studies revealed that the structural changes, such as the substitution of the phenyl ring, the modification of the heteroaromatic ring, and the connecting position of the ring relative to the azo group, significantly affect the performance of the novel azobenzene class.[230–234] By tuning the heteroaromatic ring, the half-lives of *cis*-azoheteroarene compounds could be tuned from seconds to minutes, hours, days and even to years. Due to the large tunability of half-lives,

and the predictable properties, it is expected that the azoheteroaryl photoswitches will show promising characteristics in the area of Azo-STF applications.

4.3 Solar thermal fuels covering full solar spectrum

The charging of Azo-STFs that have been reported usually requires UV irradiation. However, sunlight contains only about 5% UV light, which severely limits the Azo-STF efficiency. Besides, the organic materials could be damaged by some UV-induced side reactions. It is very important to develop novel Azo-STF materials that could respond to visible and near-infrared light. However, visible light poses an obstacle to the energy storage of Azo-STFs because it can reverse the charge process by converting the high-energy *cis*-isomers back to low-energy *trans*-isomers. Therefore, the fabrication of Azo-STFs that can operate efficiently under full-spectrum solar irradiation is fascinating but also challenging.

In the past few years, researchers have successfully designed diverse azobenzene photoswitches that could be stimulated with visible and infrared light.[235–247] These azobenzene molecules are mainly applied to biological fields such as in optically controlled drug delivery, photocontrolled ion channels, and biomolecular structures in intracellular environments.[248–250] With these existing studies, it may be possible to have an enlightening effect on the molecular design of STF-related applications.

It has been well documented that introducing substituents to azobenzene could change its absorption bands.[81] Previous studies showed that EDGs (such as $-NH_2$ and $-OH$) substituted at the *para*-position of azobenzene could shift the absorption band to longer wavelengths, and the order of the increasing red-shift effect is $H < OH < NH_2 < N(CH_3)_2$.[251] The 4-donor–4′-acceptor-substituted azobenzene (push–pull Azo) usually has a long wavelength absorption, which is caused by a push–pull system with an EDG on one side of the azobenzene and an EWG on the other.[252] Additionally, many studies introduced such push–pull Azos into polymer films through supramolecular interactions.[253–255] Although the absorption bands of supramolecular azopolymers are tunable, the half-lives of such materials largely depend on the type of substituents and solvents. This may prove difficult in practical applications.

Researchers have reported some examples of newly designed azobenzene photoswitches in recent years that can be fully photoconverted with visible light. Fig. 23 lists the maximum irradiation wavelengths for isomerization of different types of azobenzene. The first examples, a tetra-*ortho*-methoxy (**27**) and an ethylene-bridged azobenzene (**22**), described by Woolley *et al.*[256] and Herges *et al.*,[156] respectively, were based on the same strategy of separating the n–π* transitions of the *cis* and *trans* isomers. The split of the two n–π* absorption bands allowed their application to trigger both forward and reverse isomerization under visible-light irradiation. In the meantime, the π–π* band in the UV region could induce the *cis*-to-*trans* isomerization. Beyond that, Herges's group successfully synthesized oxygen and sulfur-bridged azobenzenes, as illustrated in Fig. 23 (**25**).[223] These two azobenzene derivatives could be switched with a far-red (650 nm) light source. Compared to the pristine br-Azo, the sulfur system exhibited higher thermal stability of 3.5 days. The superior photophysical properties of the sulfur-bridged azobenzene system make it an ideal candidate for STF materials. For decades, Woolley and co-workers have been devoted to the exploration of azobenzene-based photoswitching that was employed to control biomolecular targets such as proteins, peptides, and nucleic acids *in vitro* and in cell extracts through photostimulation.[86,248–258] As a result, tetra-*ortho*-substituted azobenzenes with bulky EDGs such as Cl and Br atoms and thioether groups were synthesized, with which they can be effectively isomerized under red light irradiation (**26**). All these studies proved that the absorption bands could be tuned by changing the tetra-*ortho*-substituted groups; thus, we can use this utility tool to develop extended versions of the Azo-STF application.

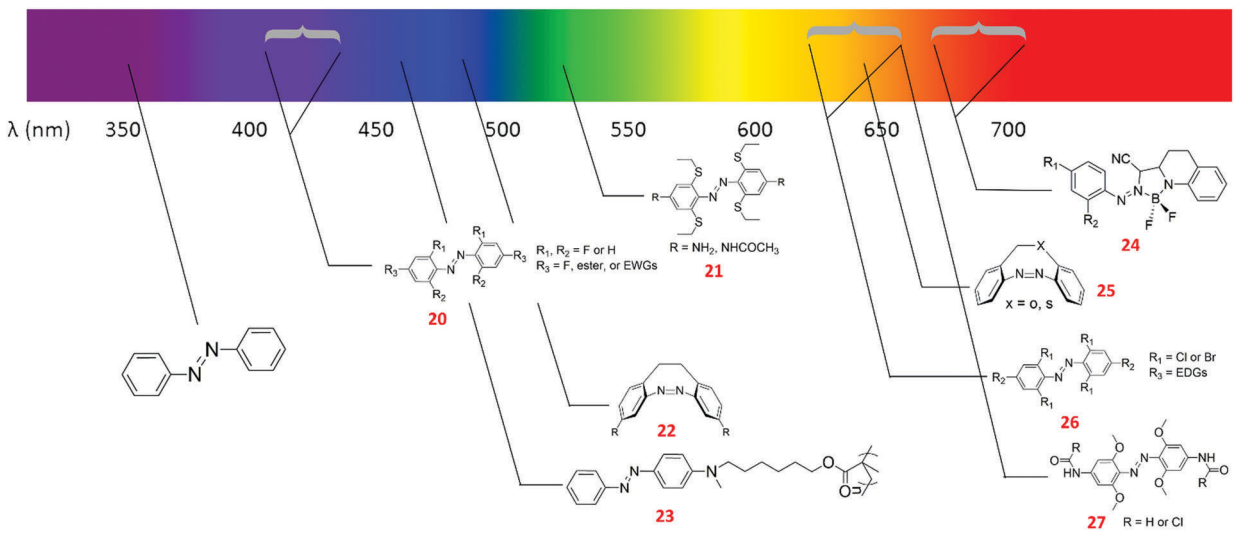

Fig. 23 Maximum irradiation wavelength for isomerization of different types of azobenzene.

Later, Aprahamian and co-workers reported a new type of azobenzene, namely BF_2-coordinated azobenzene, in which the positions of π–π* and n–π* transition energy levels were reversed, allowing the conversion of *trans*-Azo to *cis*-Azo under visible light.[259] Further, density functional theory calculations indicated that an increase in electron density could red-shift the absorption bands in the system. The authors verified the hypothesis by grafting EDGs onto *para*- and *ortho*-positions of BF_2-Azo (Fig. 23, **24**).[260,261] Altering the R_1 and R_2 groups enabled the shifting of absorption bands to the red and even near infrared regions. However, Bai *et al.*[262] found that with an increase in electron-donating ability, the thermal *cis*-to-*trans* isomerization rates were accelerated, and therefore, the corresponding half-lives were shortened.

Much progress has been achieved in tuning the long wavelength photoconversion of azobenzene as shown in Fig. 23. Various strategies, which rely on separating the n–π* bands in the visible range or red-shifting the π–π* transition absorption band, have been applied to accomplish this target, including: (i) the introduction of EWGs or EDGs at the *ortho* or *para* position, (ii) the use of a push–pull system, and (iii) the utilization of bridged azobenzene, tetra-*ortho*-position substituted azobenzene, and BF_2-coordinated azobenzene derivatives. In general, shifting the absorption bands of azobenzene to longer wavelengths often results in a fast *cis*-to-*trans* thermal isomerization, which is undesirable for STF application.[263,264] Thus, sometimes, some small compromises need to be made to balance this conflict, thereby achieving the maximum solar energy capacity and conversion efficiency.

Apart from this, other red-shifted azobenzene derivatives are also used for photocontrol.[249,258,265–268] However, we did not discuss these compounds here because they contain too many undesirable groups that cause a huge reduction in thermal stability or ED. We can summarize the general principle of designing full-spectrum STFs in that the target azobenzene can be switched upon visible-light irradiation without enhancing the thermal isomerization rate.

5. Conclusions and perspectives

In conclusion, azobenzene-based solar thermal fuels have been proven to be a promising and efficient pathway for solar-thermal conversion and storage solutions. In this context, pure azobenzene derivatives, nanocarbon-templated azobenzene, and polymer-templated azobenzene have attracted increasing attention over the past few years. However, the fast-growing research field is restricted by low ED, low quantum yield, short half-life, narrow overlap with the solar spectrum, and irreversible degradation. Much effort has been devoted by researchers to counterbalance these shortcomings of Azo-STF materials, such as by grafting functional chemical groups to improve the ED and thermal stability, combining PCMs or carbon nanomaterials to facilitate practical applications of the materials, and tuning the microstructures of the monomers and polymer backbones to maximize the absorption efficiency. Undoubtedly, molecular design engineering and microstructure optimization are paramount for achieving Azo-STFs with high-energy storage capacities. To realize the practical applications of Azo-STFs, the following criteria, *i.e.*, ''three high and three low,'' should be fulfilled: (i) The storage energy density ($\Delta H_{storage}$) must be as high as possible. (ii) The photoisomerization degree from *trans*-Azo to *cis*-Azo should be high to increase the heat release. (iii) The energy barrier (ΔE_a) from *cis*-Azo to *trans*-Azo should be high enough to enable the necessary long-term storage. (iv) The absorption spectrum should be optimized with respect to the solar emission spectrum to achieve maximal efficiency. In other words, maximum light absorption efficiency should be achieved with minimum illumination. (v) The photoactive materials should exhibit low degradation and strong cyclability performance to satisfy the stability requirements even under the extreme circumstances such as high temperatures, freezing cold, strong acidity, high salinity, *etc.* (vi) The cost of the Azo-STF materials must be competitive.

However, achieving simultaneous improvements in ED, energy barriers, and absorption efficiency, restraining degradation, and reducing cost are still a challenging task. For example, the *trans* form of azobenzene photoswitches cannot be fully converted into the *cis* form under unfiltered sunlight. It is of paramount importance to develop a very facile and more general methodology for the fabrication of Azo-STFs that work efficiently under full-spectrum solar irradiation in the future. A large red-shift in the absorption wavelength of azobenzene photoswitches is required to achieve full-spectrum Azo-STFs, but it inevitably leads to undesirable reduction in ED and thermal stability. Therefore, to accomplish the maximum solar energy capacity and conversion efficiency, we should make a trade-off between different parameters of Azo-STFs such as ED, lifetime, and absorption efficiency. Besides, it is also very important to further explore the underlying mechanisms of STF materials such as EDG/EWG substituents, steric configuration, grafting density, and inter- or intra-molecular interaction. It should be noted that the field of Azo-STFs is still in its nascent stage. New methods for preparing Azo-STF materials should be developed such as controlled self-assembly, electrospinning, electropolymerization, 3D printing, injection molding, and calendar molding. Future investigations of solid-state Azo-STFs could allow the possibility of integrating them into various existing solid-state devices for deicing, seawater desalination, manufacturing salt, and in thermal-driven generators. Azo-STFs could also find important applications in both military and consumer-oriented areas such as deep space probes, thermal power systems, temperature control systems in space stations, warm clothing, solar blankets, thermal-powered cars, and solar water heaters. Additionally, future research can present infinite golden opportunities. For example, the combination of Azo-STFs with directional heat-conduction materials afforded directional transport of heat energy. The combination of Azo-STFs with thermoelectric materials may enhance the thermoelectric figure of merit (ZT). In summary, there is much room for improvement of Azo-STFs in terms of fundamental theory and practical applications. There is no doubt that Azo-STFs pave new avenues

for solar energy harvesting and storage. High ED, long storage lifetime, controllable heat release, and outstanding cycling stability have been and will continue to be hot topics in the area of Azo-STFs. Future investigations of these promising topics with infinite possibilities will not only broaden our knowledge of Azo-STFs, but also promote their diverse applications as solar energy harvesting and storage materials.

Conflicts of interest

There are no conflicts to declare.

Acknowledgements

This work was financially supported by the National Natural Science Funds for Distinguished Young Scholars (No. 51425306), the State Key Program of National Natural Science Foundation of China (No. 51633007), the National Key R&D Program of China (No. 2016YFA0202302), and the National Natural Science Foundation of China (No. 51573125 and 51573147). W.F. designed and supervised the project; L. Q. D. and L. W. investigated and wrote the original draft; L. Q. D., Y. Y. F., L. W. and W. F. checked the manuscript in detail. The authors sincerely appreciate the anonymous referees for valuable suggestions.

Notes and references

1 A. Nicola and B. Vincenzo, *Angew. Chem., Int. Ed.*, 2007, **46**, 52–66.
2 M. Perez and R. Perez, *IEA-SHCP-Newsletter*, 2015, vol. 62, pp. 4–6.
3 T. R. Cook, D. K. Dogutan, S. Y. Reece, Y. Surendranath, T. S. Teets and D. G. Nocera, *Chem. Rev.*, 2010, **110**, 6474–6502.
4 I. Dincer, *Renewable Sustainable Energy Rev.*, 2000, **4**, 157–175.
5 D. Abbott, *Proc. IEEE*, 2010, **98**, 42–66.
6 T. J. Kucharski, Y. C. Tian, S. Akbulatov and R. Boulatov, *Energy Environ. Sci.*, 2011, **4**, 4449–4472.
7 X. Huang, X. Y. Qi, F. Boey and H. Zhang, *Chem. Soc. Rev.*, 2012, **41**, 666–686.
8 S. Gunes, H. Neugebauer and N. S. Sariciftci, *Chem. Rev.*, 2007, **107**, 1324–1338.
9 J. S. Wu, S. W. Cheng, Y. J. Cheng and C. S. Hsu, *Chem. Soc. Rev.*, 2015, **44**, 1113–1154.
10 H. A. Atwater and A. Polman, *Nat. Mater.*, 2010, **9**, 205–213.
11 M. M. Lee, J. Teuscher, T. Miyasaka, T. N. Murakami and H. J. Snaith, *Science*, 2012, **338**, 643–647.
12 M. Z. Liu, M. B. Johnston and H. J. Snaith, *Nature*, 2013, **501**, 395–398.
13 M. Graetzel, R. A. J. Janssen, D. B. Mitzi and E. H. Sargent, *Nature*, 2012, **488**, 304–312.
14 R. A. Janssen and N. Jenny, *Adv. Mater.*, 2013, **25**, 1847–1858.
15 S. A. Kalogirou, *Prog. Energy Combust. Sci.*, 2004, **30**, 231–295.
16 C. G. Granqvist, *Sol. Energy Mater. Sol. Cells*, 2007, **91**, 1529–1598.
17 Z. A. A. Majid, M. Y. Othman, M. H. Ruslan, S. Mat, B. Ali, A. Zaharim and K. Sopian, *Energy Environ. Eng. S.*, 2009, pp. 342–346.
18 A. Fernandez-Garcia, E. Zarza, L. Valenzuela and M. Perez, *Renewable Sustainable Energy Rev.*, 2010, **14**, 1695–1721.
19 T. P. Otanicar, P. E. Phelan, R. S. Prasher, G. Rosengarten and R. A. Taylor, *J. Renewable Sustainable Energy*, 2010, **2**, 033102.
20 Y. Tian and C. Y. Zhao, *Appl. Energy*, 2013, **104**, 538–553.
21 D. A. Baharoon, H. A. Rahman, W. Z. W. Omar and S. O. Fadhl, *Renewable Sustainable Energy Rev.*, 2015, **41**, 996–1027.
22 J. Barber, *Chem. Soc. Rev.*, 2009, **38**, 185–196.
23 V. Balzani, A. Credi and M. Venturi, *ChemSusChem*, 2008, **1**, 26–58.
24 Y. Ma, X. L. Wang, Y. S. Jia, X. B. Chen, H. X. Han and C. Li, *Chem. Rev.*, 2014, **114**, 9987–10043.
25 T. R. Cook, D. K. Dogutan, S. Y. Reece, Y. Surendranath, T. S. Teets and D. G. Nocera, *Chem. Rev.*, 2010, **110**, 6474–6502.
26 Y. Liu and J. C. Grossman, *Nano Lett.*, 2014, **14**, 7046–7050.
27 A. Lennartson, A. Roffey and K. Moth-Poulsen, *Tetrahedron Lett.*, 2015, **56**, 1457–1465.
28 G. Jones, T. E. Reinhardt and W. R. Bergmark, *Sol. Energy*, 1978, **20**, 241–248.
29 G. Jones, S. H. Chiang and P. T. Xuan, *J. Photochem.*, 1979, **10**, 1–18.
30 Z. Yoshida, *J. Photochem.*, 1985, **29**, 27–40.
31 D. Donati, G. Guarini and P. Sarti-fantoni, *Mol. Cryst. Liq. Cryst.*, 1972, **17**, 187–195.
32 G. Guarini and P. Sarti-Fantoni, *Mol. Cryst.*, 1970, **6**, 423.
33 J. H. Kim, F. Deng, F. N. Castellano and J. H. Kim, *ACS Photonics*, 2014, **1**, 382–388.
34 R. R. Islangulov and F. N. Castellano, *Angew. Chem., Int. Ed.*, 2006, **45**, 5957–5959.
35 D. V. Kozlov and F. N. Castellano, *Chem. Commun.*, 2004, 2860–2861.
36 R. R. Islangulov, D. V. Kozlov and F. N. Castellano, *Chem. Commun.*, 2005, 3776–3778.
37 T. N. Singh-Rachford, J. Lott, C. Weder and F. N. Castellano, *J. Am. Chem. Soc.*, 2009, **131**, 12007–12014.
38 R. Vadrucci, C. Weder and Y. C. Simon, *Mater. Horiz.*, 2015, **2**, 120–124.
39 N. Kimizuka, N. Yanai and M. Morikawa, *Langmuir*, 2016, **32**, 12304–12322.
40 D. H. Waldeck, *Chem. Rev.*, 1991, **91**, 415–436.
41 J. M. Hicks, M. T. Vandersall, E. V. Sitzmann and K. B. Eisenthal, *Chem. Phys. Lett.*, 1987, **135**, 413–420.
42 V. Caia, G. Cum, R. Gallo, V. Mancini and E. Pitoni, *Tetrahedron Lett.*, 1983, **24**, 3903–3904.
43 C. Bastianelli, V. Caia, G. Cum, R. Gallo and V. Mancini, *J. Chem. Soc., Perkin Trans. 2*, 1991, 679–683.
44 D. Schulte-Frohlinde, H. Blume and H. Güsten, *J. Phys. Chem.*, 1962, **66**, 2486–2491.
45 K. P. C. Vollhardt and T. W. Weidman, *J. Am. Chem. Soc.*, 1983, **105**, 1676–1677.

46 K. P. C. Vollhardt and T. W. Weidman, *Organometallics*, 1984, **3**, 82–86.
47 R. Boese, J. K. Cammack, A. J. Matzger, K. Pflug, W. B. Tolman, K. P. C. Vollhardt and T. W. Weidman, *J. Am. Chem. Soc.*, 1997, **119**, 6757–6773.
48 Y. Kanai, V. Srinivasan, S. K. Meier, K. P. C. Vollhardt and J. C. Grossman, *Angew. Chem., Int. Ed.*, 2010, **49**, 8926–8929.
49 J. Cho, L. Berbil-Bautista, I. V. Pechenezhskiy, N. Levy, S. K. Meier, V. Srinivasan, Y. Kanai, J. C. Grossman, K. P. C. Vollhardt and M. F. Crommie, *ACS Nano*, 2011, **5**, 3701–3706.
50 K. Moth-Poulsen, D. Coso, K. Borjesson, N. Vinokurov, S. K. Meier, A. Majumdar, K. P. C. Vollhardt and R. A. Segalman, *Energy Environ. Sci.*, 2012, **5**, 8534–8537.
51 Z. R. Hou, S. C. Nguyen, J. P. Lomont, C. B. Harris, N. Vinokurov and K. P. C. Vollhardt, *Phys. Chem. Chem. Phys.*, 2013, **15**, 7466–7469.
52 K. Borjesson, D. Coso, V. Gray, J. C. Grossman, J. Q. Guan, C. B. Harris, N. Hertkorn, Z. R. Hou, Y. Kanai, D. Lee, J. P. Lomont, A. Majumdar, S. K. Meier, K. Moth-Poulsen, R. L. Myrabo, S. C. Nguyen, R. A. Segalman, V. Srinivasan, W. B. Tolman, N. Vinokurov, K. P. C. Vollhardt and T. W. Weidman, *Chem. – Eur. J.*, 2014, **20**, 15587–15604.
53 K. Borjesson, A. Lennartson and K. Moth-Poulsen, *J. Fluorine Chem.*, 2014, **161**, 24–28.
54 B. Zhu, O. Š. Miljanić, K. P. C. Vollhardt and M. J. West, *Synthesis*, 2005, 3373–3379.
55 C. Philippopoulos, D. Economou, C. Economou and J. Marangozis, *Ind. Eng. Chem. Prod. Res. Dev.*, 1983, **22**, 627–633.
56 V. Gray, A. Lennartson, P. Ratanalert, K. Borjesson and K. Moth-Poulsen, *Chem. Commun.*, 2014, **50**, 5330–5332.
57 O. Brummel, D. Besold, T. Dopper, Y. L. Wu, S. Bochmann, F. Lazzari, F. Waidhas, U. Bauer, P. Bachmann, C. Papp, H. P. Steinruck, A. Gorling, J. Libuda and J. Bachmann, *ChemSusChem*, 2016, **9**, 1424–1432.
58 M. Kuisma, A. Lundin, K. Moth-Poulsen, P. Hyldgaard and P. Erhart, *ChemSusChem*, 2016, **9**, 1786–1794.
59 M. J. Kuisma, A. M. Lundin, K. Moth-Poulsen, P. Hyldgaard and P. Erhart, *J. Phys. Chem. C*, 2016, **120**, 3635–3645.
60 O. Brummel, F. Waidhas, U. Bauer, Y. L. Wu, S. Bochmann, H. P. Steinruck, C. Papp, J. Bachmann and J. Libuda, *J. Phys. Chem. Lett.*, 2017, **8**, 2819–2825.
61 A. Dreos, K. Borjesson, Z. H. Wang, A. Roffey, Z. Norwood, D. Kushnir and K. Moth-Poulsen, *Energy Environ. Sci.*, 2017, **10**, 728–734.
62 J. Gurke, M. Quick, N. P. Ernsting and S. Hecht, *Chem. Commun.*, 2017, **53**, 2150–2153.
63 K. Jorner, A. Dreos, R. Emanuelsson, O. El Bakouri, I. F. Galvan, K. Borjesson, F. Feixas, R. Lindh, B. Zietz, K. Moth-Poulsen and H. Ottosson, *J. Mater. Chem. A*, 2017, **5**, 12369–12378.
64 V. A. Bren, D. D. Alexander, I. M. Vladimir and V. A. Chernoivanov, *Russ. Chem. Rev.*, 1991, **60**, 451–469.
65 D. D. Alexander, A. B. Vladimir and V. A. Chernoivanov, *Russ. Chem. Rev.*, 2002, **71**, 917–927.
66 H. Goerner, C. Fischer, S. Gierisch and J. Daub, *J. Phys. Chem.*, 1993, **97**, 4110–4117.
67 H. Görner, C. Fischer and J. Daub, *J. Photochem. Photobiol., A*, 1995, **85**, 217–224.
68 A. Plaquet, B. Champagne, F. Castet, L. Ducasse, E. Bogdan, V. Rodriguez and J.-L. Pozzo, *New J. Chem.*, 2009, **33**, 1349–1356.
69 S. Lara-Avila, A. V. Danilov, S. E. Kubatkin, S. L. Broman, C. R. Parker and M. B. Nielsen, *J. Phys. Chem. C*, 2011, **115**, 18372–18377.
70 S. L. Broman, S. Lara-Avila, C. L. Thisted, A. D. Bond, S. Kubatkin, A. Danilov and M. B. Nielsen, *Adv. Funct. Mater.*, 2012, **22**, 4249–4258.
71 A. Vlasceanu, S. L. Broman, A. S. Hansen, A. B. Skov, M. Cacciarini, A. Kadziola, H. G. Kjaergaard, K. V. Mikkelsen and M. B. Nielsen, *Chem. – Eur. J.*, 2016, **22**, 10796–10800.
72 A. B. Skov, S. L. Broman, A. S. Gertsen, J. Elm, M. Jevric, M. Cacciarini, A. Kadziola, K. V. Mikkelsen and M. B. Nielsen, *Chem. – Eur. J.*, 2016, **22**, 14567–14575.
73 A. B. Skov, J. F. Petersen, J. Elm, B. N. Frandsen, M. Santella, M. D. Kilde, H. G. Kjaergaard, K. V. Mikkelsen and M. B. Nielsen, *ChemPhotoChem*, 2017, **1**, 206–212.
74 Z. H. Wang, J. Udmark, K. Borjesson, R. Rodrigues, A. Roffey, M. Abrahamsson, M. B. Nielsen and K. Moth-Poulsen, *ChemSusChem*, 2017, **10**, 3049–3055.
75 M. Cacciarini, A. Vlasceanu, M. Jevric and M. B. Nielsen, *Chem. Commun.*, 2017, **53**, 5874–5877.
76 A. Vlasceanu, B. N. Frandsen, A. B. Skov, A. S. Hansen, M. G. Rasmussen, H. G. Kjaergaard, K. V. Mikkelsen and M. B. Nielsen, *J. Org. Chem.*, 2017, **82**, 10398–10407.
77 S. L. Broman, M. Jevric, A. D. Bond and M. B. Nielsen, *J. Org. Chem.*, 2014, **79**, 41–64.
78 T. J. Kucharski, N. Ferralis, A. M. Kolpak, J. O. Zheng, D. G. Nocera and J. C. Grossman, *Nat. Chem.*, 2014, **6**, 441–447.
79 W. Feng, W. Luo and Y. Y. Feng, *Nanoscale*, 2012, **4**, 6118–6134.
80 A. K. Saydjari, P. Weis and S. Wu, *Adv. Energy Mater.*, 2017, **7**, 1601622.
81 H. M. Bandara and S. C. Burdette, *Chem. Soc. Rev.*, 2012, **41**, 1809–1825.
82 H. Zollinger, *Color Chemistry: Syntheses, Properties, and Applications of Organic Dyes and Pigments*, Wiley-VCH, 2003.
83 G. S. Hartley, *Nature*, 1937, **140**, 281.
84 E. Merino, *Chem. Soc. Rev.*, 2011, **40**, 3835–3853.
85 D. Wang and X. Wang, *Prog. Polym. Sci.*, 2013, **38**, 271–301.
86 A. A. Beharry and G. A. Woolley, *Chem. Soc. Rev.*, 2011, **40**, 4422–4437.
87 L. F. Wu, X. L. Tuo, H. Cheng, Z. Chen and X. G. Wang, *Macromolecules*, 2001, **34**, 8005–8013.
88 Y. N. He, X. G. Wang and Q. X. Zhou, *Polymer*, 2002, **43**, 7325–7333.
89 B. Priewisch and K. Ruck-Braun, *J. Org. Chem.*, 2005, **70**, 2350–2352.
90 T. Gunnlaugsson, J. P. Leonard and N. S. Murray, *Org. Lett.*, 2004, **6**, 1557–1560.
91 X. J. Zhou, T. Zifer, B. M. Wong, K. L. Krafcik, F. Leonard and A. L. Vance, *Nano Lett.*, 2009, **9**, 1028–1033.

92 Y. L. Yu, M. Nakano and T. Ikeda, *Nature*, 2003, **425**, 145.
93 N. Hosono, T. Kajitani, T. Fukushima, K. Ito, S. Sasaki, M. Takata and T. Aida, *Science*, 2010, **330**, 808–811.
94 C. Q. Qin, Y. Y. Feng, W. Luo, C. Cao, W. P. Hu and W. Feng, *J. Mater. Chem. A*, 2015, **3**, 16453–16460.
95 H. K. Bisoyi and Q. Li, *Chem. Rev.*, 2016, **116**, 15089–15166.
96 J. A. Delaire and K. Nakatani, *Chem. Rev.*, 2000, **100**, 1817–1845.
97 Z. G. Zheng, Y. N. Li, H. K. Bisoyi, L. Wang, T. J. Bunning and Q. Li, *Nature*, 2016, **531**, 352–356.
98 L. Wang, D. Chen, K. G. Gutierrez-Cuevas, H. K. Bisoyi, J. Fan, R. S. Zola, G. Q. Li, A. M. Urbas, T. J. Bunning, D. A. Weitz and Q. Li, *Mater. Horiz.*, 2017, **4**, 1190–1195.
99 R. Hagen and T. Bieringer, *Adv. Mater.*, 2001, **13**, 1805–1810.
100 P. O. Astrand, P. S. Ramanujam, S. Hvilsted, K. L. Bak and S. P. A. Sauer, *J. Am. Chem. Soc.*, 2000, **122**, 3482–3487.
101 A. S. Matharu, S. Jeeva and P. S. Ramanujam, *Chem. Soc. Rev.*, 2007, **36**, 1868–1880.
102 J. Olmsted, J. Lawrence and G. G. Yee, *Sol. Energy*, 1983, **30**, 271–274.
103 H. Taoda, K. Hayakawa, K. Kawase and H. Yamakita, *J. Chem. Eng. Jpn.*, 1987, **20**, 265–270.
104 H. K. Bisoyi and Q. Li, *Acc. Chem. Res.*, 2014, **47**, 3184–3195.
105 L. Wang and Q. Li, *Chem. Soc. Rev.*, 2018, **47**, 1044–1097.
106 E. N. Cho, PhD thesis, Massachusetts Institute of Technology, 2017.
107 X. Wang, *Azo Polymers, Synthesis, Functions and Applications*, Springer Berlin Heidelberg, 2017.
108 C. R. Crecca and A. E. Roitberg, *J. Phys. Chem. A*, 2006, **110**, 8188–8203.
109 C. W. Chang, Y. C. Lu, T. T. Wang and E. W. G. Diau, *J. Am. Chem. Soc.*, 2004, **126**, 10109–10118.
110 T. Ishikawa, T. Noro and T. Shoda, *J. Chem. Phys.*, 2001, **115**, 7503–7512.
111 P. Cattaneo and M. Persico, *Phys. Chem. Chem. Phys.*, 1999, **1**, 4739–4743.
112 T. Schultz, J. Quenneville, B. Levine, A. Toniolo, T. J. Martinez, S. Lochbrunner, M. Schmitt, J. P. Shaffer, M. Z. Zgierski and A. Stolow, *J. Am. Chem. Soc.*, 2003, **125**, 8098–8099.
113 C. Ciminelli, G. Granucci and M. Persico, *Chem. – Eur. J.*, 2004, **10**, 2327–2341.
114 C. M. Stuart, R. R. Frontiera and R. A. Mathies, *J. Phys. Chem. A*, 2007, **111**, 12072–12080.
115 I. Conti, M. Garavelli and G. Orlandi, *J. Am. Chem. Soc.*, 2008, **130**, 5216–5230.
116 G. Tiberio, L. Muccioli, R. Berardi and C. Zannoni, *ChemPhysChem*, 2010, **11**, 1018–1028.
117 J. Azuma, N. Tamai, A. Shishido and T. Ikeda, *Chem. Phys. Lett.*, 1998, **288**, 77–82.
118 I. K. Lednev, T. Q. Ye, P. Matousek, M. Towrie, P. Foggi, F. V. R. Neuwahl, S. Umapathy, R. E. Hester and J. N. Moore, *Chem. Phys. Lett.*, 1998, **290**, 68–74.
119 T. Fujino and T. Tahara, *J. Phys. Chem. A*, 2000, **104**, 4203–4210.
120 H. Satzger, S. Spörlein, C. Root, J. Wachtveitl, W. Zinth and P. Gilch, *Chem. Phys. Lett.*, 2003, **372**, 216–223.
121 Y. C. Lu, E. W. G. Diau and H. Rau, *J. Phys. Chem. A*, 2005, **109**, 2090–2099.
122 K. Börjesson, A. Lennartson and K. Moth-Poulsen, *ACS Sustainable Chem. Eng.*, 2013, **1**, 585–590.
123 A. W. Adamson, A. Vogler, H. Kunkely and R. Wachter, *J. Am. Chem. Soc.*, 1978, **100**, 1298–1300.
124 K. Masutani, M. Morikawa and N. Kimizuka, *Chem. Commun.*, 2014, **50**, 15803–15806.
125 E. N. Cho, D. Zhitomirsky, G. G. D. Han, Y. Liu and J. C. Grossman, *ACS Appl. Mater. Interfaces*, 2017, **9**, 8679–8687.
126 G. G. D. Han, H. S. Li and J. C. Grossman, *Nat. Commun.*, 2017, **8**, 1446.
127 S. Monti, G. Orlandi and P. Palmieri, *Chem. Phys.*, 1982, **71**, 87–99.
128 E. Durgun and J. C. Grossman, *J. Phys. Chem. Lett.*, 2013, **4**, 854–860.
129 A. M. Kolpak and J. C. Grossman, *J. Chem. Phys.*, 2013, **138**, 034303.
130 Z. Hu, D. Y. Zhang, L. Yu and Y. D. Huang, *J. Mater. Chem. B*, 2018, **6**, 518–526.
131 Y. Y. Feng, W. Feng, H. Noda, T. Sekino, A. Fujii, M. Ozaki and K. Yoshino, *Carbon*, 2007, **45**, 2445–2448.
132 Y. Y. Feng, W. Feng, H. Noda, A. Fujii, M. Ozaki, K. Yoshino and K. Yoshino, *J. Appl. Phys.*, 2007, **102**, 053102.
133 A. M. Kolpak and J. C. Grossman, *Nano Lett.*, 2011, **11**, 3156–3162.
134 X. Du, I. Skachko, F. Duerr, A. Luican and E. Y. Andrei, *Nature*, 2009, **462**, 192–195.
135 T. L. Cao, F. Y. Zhao, Z. L. Da, F. X. Qiu, D. Y. Yang, Y. J. Guan, G. R. Cao, Z. R. Zhao, J. X. Li and X. T. Guo, *Z. Phys. Chem.*, 2017, **231**, 1797–1814.
136 C. J. Xia, M. Ye, B. Q. Zhang, Y. H. Su and Z. Y. Tu, *Jpn. J. Appl. Phys.*, 2017, **56**, 105101.
137 J. Zhao, C. Y. Liu and J. Ma, *Nanoscale*, 2017, **9**, 19017–19025.
138 S. C. Shekar and R. S. Swathi, *Carbon*, 2018, **126**, 489–499.
139 M. Li, Y. Y. Feng, E. Z. Liu, C. Q. Qin and W. Feng, *Sci. China: Technol. Sci.*, 2016, **59**, 1383–1390.
140 Y. Y. Feng, H. P. Liu, W. Luo, E. Z. Liu, N. Q. Zhao, K. Yoshino and W. Feng, *Sci. Rep.*, 2013, **3**, 3260.
141 W. Luo, Y. Y. Feng, C. Cao, M. Li, E. Z. Liu, S. P. Li, C. Q. Qin, W. P. Hu and W. Feng, *J. Mater. Chem. A*, 2015, **3**, 11787–11795.
142 W. Luo, Y. Y. Feng, C. Q. Qin, M. Li, S. P. Li, C. Cao, P. Long, E. Z. Liu, W. P. Hu, K. Yoshino and W. Feng, *Nanoscale*, 2015, **7**, 16214–16221.
143 W. Feng, S. P. Li, M. Li, C. Q. Qin and Y. Y. Feng, *J. Mater. Chem. A*, 2016, **4**, 8020–8028.
144 X. Z. Zhao, Y. Y. Feng, C. Q. Qin, W. X. Yang, Q. Y. Si and W. Feng, *ChemSusChem*, 2017, **10**, 1395–1404.
145 D. Bleger, J. Dokic, M. V. Peters, L. Grubert, P. Saalfrank and S. Hecht, *J. Phys. Chem. B*, 2011, **115**, 9930–9940.
146 J. Bahrenburg, C. M. Sievers, J. B. Schonborn, B. Hartke, F. Renth, F. Temps, C. Nather and F. D. Sonnichsen, *Photochem. Photobiol. Sci.*, 2013, **12**, 511–518.
147 H. Wang, H. K. Bisoyi, L. Wang, A. M. Urbas, T. J. Bunning and Q. Li, *Angew. Chem., Int. Ed.*, 2018, **57**, 1627–1631.

148 D. Zhitomirsky, E. Cho and J. C. Grossman, *Adv. Energy Mater.*, 2016, **6**, 1502006.
149 Y. Q. Shen and H. Rau, *Makromol. Chem.*, 1991, **192**, 945–957.
150 M. Schönhoff, M. Mertesdorf and M. Lösche, *J. Phys. Chem.*, 1996, **100**, 7558–7565.
151 S. P. Jeong, L. A. Renna, C. J. Boyle, H. S. Kwak, E. Harder, W. Damm and D. Venkataraman, *Sci. Rep.*, 2017, **7**, 17773.
152 D. Zhitomirsky and J. C. Grossman, *ACS Appl. Mater. Interfaces*, 2016, **8**, 26319–26325.
153 K. Ishiba, M. Morikawa, C. Chikara, T. Yamada, K. Iwase, M. Kawakita and N. Kimizuka, *Angew. Chem., Int. Ed.*, 2015, **54**, 1532–1536.
154 G. D. Han, S. S. Park, Y. Liu, D. Zhitomirsky, E. Cho, M. Dinca and J. C. Grossman, *J. Mater. Chem. A*, 2016, **4**, 16157–16165.
155 H. W. Zhou, C. G. Xue, P. Weis, Y. Suzuki, S. L. Huang, K. Koynov, G. K. Auernhammer, R. Berger, H. J. Butt and S. Wu, *Nat. Chem.*, 2017, **9**, 145–151.
156 R. Siewertsen, H. Neumann, B. Buchheim-Stehn, R. Herges, C. Näther, F. Renth and F. Temps, *J. Am. Chem. Soc.*, 2009, **131**, 15594–15595.
157 F. Cheng, Y. Zhang, R. Yin and Y. Yu, *J. Mater. Chem.*, 2010, **20**, 4888–4896.
158 A. A. Beharry, O. Sadovski and G. A. Woolley, *J. Am. Chem. Soc.*, 2011, **133**, 19684–19687.
159 P. Weis, D. S. Wang and S. Wu, *Macromolecules*, 2016, **49**, 6368–6373.
160 K. Nishizawa, S. Nagano and T. Seki, *Chem. Mater.*, 2009, **21**, 2624–2631.
161 O. Tsutsumi, T. Kitsunai, A. Kanazawa, T. Shiono and T. Ikeda, *Macromolecules*, 1998, **31**, 355–359.
162 Y. Norikane, Y. Hirai and M. Yoshida, *Chem. Commun.*, 2011, **47**, 1770–1772.
163 E. Uchida, K. Sakaki, Y. Nakamura, R. Azumi, Y. Hirai, H. Akiyama, M. Yoshida and Y. Norikane, *Chem. – Eur. J.*, 2013, **19**, 17391–17397.
164 M. Hoshino, E. Uchida, Y. Norikane, R. Azumi, S. Nozawa, A. Tomita, T. Sato, S. Adachi and S. Y. Koshihara, *J. Am. Chem. Soc.*, 2014, **136**, 9158–9164.
165 Y. Norikane, E. Uchida, S. Tanaka, K. Fujiwara, E. Koyama, R. Azumi, H. Akiyama, H. Kihara and M. Yoshida, *Org. Lett.*, 2014, **16**, 5012–5015.
166 X. Li, B. Li, M. He, W. Wang, T. Wang, A. Wang, J. Yu, Z. Wang, S. W. Hong, M. Byun, S. Lin, H. Yu and Z. Lin, *ACS Appl. Mater. Interfaces*, 2018, **10**, 4961–4970.
167 S. J. Rowan, S. J. Cantrill, G. R. L. Cousins, J. K. M. Sanders and J. F. Stoddart, *Angew. Chem., Int. Ed.*, 2002, **41**, 898–952.
168 T. Maeda, H. Otsuka and A. Takahara, *Prog. Polym. Sci.*, 2009, **34**, 581–604.
169 Y. Jin, C. Yu, R. J. Denman and W. Zhang, *Chem. Soc. Rev.*, 2013, **42**, 6634–6654.
170 H. Xu, W. Cao and X. Zhang, *Acc. Chem. Res.*, 2013, **46**, 1647–1658.
171 M. E. Belowich and J. F. Stoddart, *Chem. Soc. Rev.*, 2012, **41**, 2003–2024.
172 N. Ma, Y. Li, H. Xu, Z. Wang and X. Zhang, *J. Am. Chem. Soc.*, 2010, **132**, 442–443.
173 Y. Yi, H. Xu, L. Wang, W. Cao and X. Zhang, *Chem. – Eur. J.*, 2013, **19**, 9506–9510.
174 X. Huang, R. Fang, D. Wang, J. Wang, H. Xu, Y. Wang and X. Zhang, *Small*, 2015, **11**, 1537–1541.
175 D. Chen, D. Wang, Y. Yang, Q. Huang, S. Zhu and Z. Zheng, *Adv. Energy Mater.*, 2017, **7**, 1700890.
176 R. J. Wojtecki, M. A. Meador and S. J. Rowan, *Nat. Mater.*, 2010, **10**, 14.
177 N. K. Kildahl, *J. Chem. Educ.*, 1995, **72**, 423.
178 K. Stranius and K. Borjesson, *Sci. Rep.*, 2017, **7**, 41145.
179 T. Fujino, S. Y. Arzhantsev and T. Tahara, *J. Phys. Chem. A*, 2001, **105**, 8123–8129.
180 E. Fischer, M. Frankel and R. Wolovsky, *J. Chem. Phys.*, 1955, **23**, 1367.
181 P. Bortolus and S. Monti, *J. Phys. Chem.*, 1979, **83**, 648–652.
182 N. Siampiringue, G. Guyot, S. Monti and P. Bortolus, *J. Photochem.*, 1987, **37**, 185–188.
183 D. Gegiou, K. A. Muszkat and E. Fischer, *J. Am. Chem. Soc.*, 1968, **90**, 12–18.
184 S. G. Mayer, C. L. Thomsen, M. P. Philpott and P. J. Reid, *Chem. Phys. Lett.*, 1999, **314**, 246–254.
185 H. Rau and E. Lueddecke, *J. Am. Chem. Soc.*, 1982, **104**, 1616–1620.
186 M. Hagiri, N. Ichinose, C. Zhao, H. Horiuchi, H. Hiratsuka and T. Nakayama, *Chem. Phys. Lett.*, 2004, **391**, 297–301.
187 H. B. Zhang and M. Barra, *J. Phys. Org. Chem.*, 2005, **18**, 498–503.
188 E. Fischer, *J. Am. Chem. Soc.*, 1960, **82**, 3249–3252.
189 S. Malkin and E. Fischer, *J. Phys. Chem.*, 1962, **66**, 2482–2486.
190 K. Yoshii, S. Machida and K. Horie, *J. Polym. Sci., Part B: Polym. Phys.*, 2000, **38**, 3098–3105.
191 T. Asano, T. Yano and T. Okada, *J. Am. Chem. Soc.*, 1982, **104**, 4900–4904.
192 E. Bassotti, P. Carbone, A. Credi, M. Di Stefano, S. Masiero, F. Negri, G. Orlandi and G. P. Spada, *J. Phys. Chem. A*, 2006, **110**, 12385–12394.
193 T. Asano, T. Okada, S. Shinkai, K. Shigematsu, Y. Kusano and O. Manabe, *J. Am. Chem. Soc.*, 1981, **103**, 5161–5165.
194 I. Mita, K. Horie and K. Hirao, *Macromolecules*, 1989, **22**, 558–563.
195 Y. Yasushi, H. Hirofumi, I. Hiroshi and K. Yukio, *Bull. Chem. Soc. Jpn.*, 1990, **63**, 1607–1610.
196 T. Naito, K. Horie and I. Mita, *Macromolecules*, 1991, **24**, 2907–2911.
197 G. Pariani, A. Bianco, R. Castagna and C. Bertarelli, *J. Phys. Chem. A*, 2011, **115**, 12184–12193.
198 F. Serra and E. M. Terentjev, *Macromolecules*, 2008, **41**, 981–986.
199 A. Cembran, F. Bernardi, M. Garavelli, L. Gagliardi and G. Orlandi, *J. Am. Chem. Soc.*, 2004, **126**, 3234–3243.
200 T. Ikegami, N. Kurita, H. Sekino and Y. Ishikawa, *J. Phys. Chem. A*, 2003, **107**, 4555–4562.
201 J. Dokic, M. Gothe, J. Wirth, M. V. Peters, J. Schwarz, S. Hecht and P. Saalfrank, *J. Phys. Chem. A*, 2009, **113**, 6763–6773.

202 N. Norio, S. Toshinobu, Y. Hideyuki, I. Etsuko, Y. Shunzo and H. Shigeo, *Bull. Chem. Soc. Jpn.*, 1976, **49**, 1381–1387.
203 K. Gille, H. Knoll and K. Quitzsch, *Int. J. Chem. Kinet.*, 1999, **31**, 337–350.
204 M. Kojima, S. Nebashi, K. Ogawa and N. Kurita, *J. Phys. Org. Chem.*, 2005, **18**, 994–1000.
205 K. S. Schanze, T. F. Mattox and D. G. Whitten, *J. Org. Chem.*, 1983, **48**, 2808–2813.
206 A. A. Blevins and G. J. Blanchard, *J. Phys. Chem. B*, 2004, **108**, 4962–4968.
207 N. Biswas, B. Abraham and S. Umapathy, *J. Phys. Chem. A*, 2002, **106**, 9397–9406.
208 N. Biswas and S. Umapathy, *J. Chem. Phys.*, 2003, **118**, 5526–5536.
209 B. Schmidt, C. Sobotta, S. Malkmus, S. Laimgruber, M. Braun, W. Zinth and P. Gilch, *J. Phys. Chem. A*, 2004, **108**, 4399–4404.
210 H. Duval, *Bull. Soc. Chim. Fr.*, 1910, **7**, 727–732.
211 H. Sell, C. Näther and R. Herges, *Beilstein J. Org. Chem.*, 2013, **9**, 1–7.
212 E. Tauer and R. Machinek, *Liebigs Ann.*, 1996, **1996**, 1213–1216.
213 M. Bockmann, N. L. Doltsinis and D. Marx, *Angew. Chem., Int. Ed.*, 2010, **49**, 3382–3384.
214 O. Carstensen, J. Sielk, J. B. Schonborn, G. Granucci and B. Hartke, *J. Chem. Phys.*, 2010, **133**, 124305.
215 L. Liu, S. Yuan, W. H. Fang and Y. Zhang, *J. Phys. Chem. A*, 2011, **115**, 10027–10034.
216 N. O. Carstensen, *Phys. Chem. Chem. Phys.*, 2013, **15**, 15017–15026.
217 C. W. Jiang, R. H. Xie, F. L. Li and R. E. Allen, *J. Phys. Chem. A*, 2011, **115**, 244–249.
218 M. Bockmann, N. L. Doltsinis and D. Marx, *J. Chem. Phys.*, 2012, **137**, 22A505.
219 A. H. Gao, B. Li, P. Y. Zhang and K. L. Han, *J. Chem. Phys.*, 2012, **137**, 204305.
220 D. K. Joshi, M. J. Mitchell, D. Bruce, A. J. Lough and H. Yan, *Tetrahedron*, 2012, **68**, 8670–8676.
221 J. Cao, L. H. Liu, W. H. Fang, Z. Z. Xie and Y. Zhang, *J. Chem. Phys.*, 2013, **138**, 134306.
222 L. Liu, Y. Wang and Q. Fang, *J. Chem. Phys.*, 2017, **146**, 064308.
223 M. Hammerich, C. Schütt, C. Stähler, P. Lentes, F. Röhricht, R. Höppner and R. Herges, *J. Am. Chem. Soc.*, 2016, **138**, 13111–13114.
224 D. Bleger, J. Schwarz, A. M. Brouwer and S. Hecht, *J. Am. Chem. Soc.*, 2012, **134**, 20597–20600.
225 C. Knie, M. Utecht, F. Zhao, H. Kulla, S. Kovalenko, A. M. Brouwer, P. Saalfrank, S. Hecht and D. Bléger, *Chem. – Eur. J.*, 2014, **20**, 16492–16501.
226 C. E. Weston, R. D. Richardson, P. R. Haycock, A. J. White and M. J. Fuchter, *J. Am. Chem. Soc.*, 2014, **136**, 11878–11881.
227 J. Calbo, C. E. Weston, A. J. P. White, H. S. Rzepa, J. Contreras-García and M. J. Fuchter, *J. Am. Chem. Soc.*, 2017, **139**, 1261–1274.
228 C. E. Weston, R. D. Richardson and M. J. Fuchter, *Chem. Commun.*, 2016, **52**, 4521–4524.
229 C. E. Weston, A. Krämer, F. Colin, Ö. Yildiz, M. G. J. Baud, F. J. Meyer-Almes and M. J. Fuchter, *ACS Infect. Dis.*, 2017, **3**, 152–161.
230 J. Otsuki, K. Suwa, K. Narutaki, C. Sinha, I. Yoshikawa and K. Araki, *J. Phys. Chem. A*, 2005, **109**, 8064–8069.
231 J. Otsuki, K. Suwa, K. K. Sarker and C. Sinha, *J. Phys. Chem. A*, 2007, **111**, 1403–1409.
232 A. Kawai, D. Kawamori, T. Monji, T. Asaka, N. Akai and K. Shibuya, *Chem. Lett.*, 2010, **39**, 230–231.
233 T. Wendler, C. Schütt, C. Näther and R. Herges, *J. Org. Chem.*, 2012, **77**, 3284–3287.
234 L. Stricker, E.-C. Fritz, M. Peterlechner, N. L. Doltsinis and B. J. Ravoo, *J. Am. Chem. Soc.*, 2016, **138**, 4547–4554.
235 L. Wang, H. Dong, Y. N. Li, C. M. Xue, L. D. Sun, C. H. Yan and Q. Li, *J. Am. Chem. Soc.*, 2014, **136**, 4480–4483.
236 L. Wang, H. Dong, Y. Li, R. Liu, Y. F. Wang, H. K. Bisoyi, L. D. Sun, C. H. Yan and Q. Li, *Adv. Mater.*, 2015, **27**, 2065–2069.
237 D. Bleger and S. Hecht, *Angew. Chem., Int. Ed.*, 2015, **54**, 11338–11349.
238 M. X. Dong, A. Babalhavaeji, S. Samanta, A. A. Beharry and G. A. Woolley, *Acc. Chem. Res.*, 2015, **48**, 2662–2670.
239 W. Philipp and W. Si, *Macromol. Rapid Commun.*, 2018, **39**, 1700220.
240 W. Si and B. Hans-Jürgen, *Adv. Mater.*, 2016, **28**, 1208–1226.
241 L. Wang, K. G. Gutierrez-Cuevas, A. Urbas. and Q. Li, *Adv. Opt. Mater.*, 2016, **4**, 247–251.
242 L. Wang, K. G. Gutierrez-Cuevas, H. K. Bisoyi, J. Xiang, G. Singh, R. S. Zola, S. Kumar, O. D. Lavrentovich, A. Urbas and Q. Li, *Chem. Commun.*, 2015, **51**, 15039–15042.
243 K. G. Gutierrez-Cuevas, L. Wang, C. Xue, G. Singh, S. Kumar, A. Urbas and Q. Li, *Chem. Commun.*, 2015, **51**, 9845–9848.
244 X. Chen, L. Wang, Y. Chen, C. Li, G. Hou, X. Liu, X. Zhang, W. He and H. Yang, *Chem. Commun.*, 2014, **50**, 691–694.
245 X. Chen, L. Wang, C. Li, J. Xiao, H. Ding, X. Liu, X. Zhang, W. He and H. Yang, *Chem. Commun.*, 2013, **49**, 10097–10099.
246 Y. H. Lee, L. Wang, H. Yang and S. T. Wu, *Opt. Express*, 2015, **23**, 22658–22666.
247 L. Wang, *Liq. Cryst.*, 2016, **43**, 2062–2078.
248 O. Sadovski, A. A. Beharry, F. Zhang and G. A. Woolley, *Angew. Chem., Int. Ed.*, 2009, **48**, 1484–1486.
249 S. Samanta, A. Babalhavaeji, M. X. Dong and G. A. Woolley, *Angew. Chem., Int. Ed.*, 2013, **52**, 14127–14130.
250 S. Samanta, C. Qin, A. J. Lough and G. A. Woolley, *Angew. Chem., Int. Ed.*, 2012, **51**, 6452–6455.
251 W. R. Brode, J. H. Gould and G. M. Wyman, *J. Am. Chem. Soc.*, 1952, **74**, 4641–4646.
252 J. Griffiths, *Chem. Soc. Rev.*, 1972, **1**, 481–493.
253 J. Vapaavuori, C. G. Bazuin and A. Priimagi, *J. Mater. Chem. C*, 2018, **6**, 2168–2188.
254 S. Yagai and A. Kitamura, *Chem. Soc. Rev.*, 2008, **37**, 1520–1529.
255 A. Priimagi, G. Cavallo, A. Forni, M. Gorynsztejn-Leben, M. Kaivola, P. Metrangolo, R. Milani, A. Shishido, T. Pilati,

G. Resnati and G. Terraneo, *Adv. Funct. Mater.*, 2012, **22**, 2572–2579.
256 S. Samanta, T. M. McCormick, S. K. Schmidt, D. S. Seferos and G. A. Woolley, *Chem. Commun.*, 2013, **49**, 10314–10316.
257 S. Samanta, A. A. Beharry, O. Sadovski, T. M. McCormick, A. Babalhavaeji, V. Tropepe and G. A. Woolley, *J. Am. Chem. Soc.*, 2013, **135**, 9777–9784.
258 F. Zhang, O. Sadovski and G. A. Woolley, *ChemBioChem*, 2008, **9**, 2147–2154.
259 Y. Yang, R. P. Hughes and I. Aprahamian, *J. Am. Chem. Soc.*, 2012, **134**, 15221–15224.
260 Y. Yang, R. P. Hughes and I. Aprahamian, *J. Am. Chem. Soc.*, 2014, **136**, 13190–13193.
261 Y. Yang, X. Su, C. N. Carroll and I. Aprahamian, *Chem. Sci.*, 2012, **3**, 610–613.
262 Y. P. Wang, Z. X. Zhang, M. Xie, F. Q. Bai, P. X. Wang and H. X. Zhang, *Dyes Pigm.*, 2016, **129**, 100–108.
263 J. Garcia-Amoros and D. Velasco, *Beilstein J. Org. Chem.*, 2012, **8**, 1003–1017.
264 A. Mourot, T. Fehrentz, Y. Le Feuvre, C. M. Smith, C. Herold, D. Dalkara, F. Nagy, D. Trauner and R. H. Kramer, *Nat. Methods*, 2012, **9**, 396–412.
265 A. Rullo, A. Reiner, A. Reiter, D. Trauner, E. Y. Isacoff and G. A. Woolley, *Chem. Commun.*, 2014, **50**, 14613–14615.
266 M. Dong, A. Babalhavaeji, M. J. Hansen, L. Kalman and G. A. Woolley, *Chem. Commun.*, 2015, **51**, 12981–12984.
267 A. A. Beharry, L. Wong, V. Tropepe and G. A. Woolley, *Angew. Chem., Int. Ed.*, 2011, **50**, 1325–1327.
268 W. Wu, L. M. Yao, T. S. Yang, R. Y. Yin, F. Y. Li and Y. L. Yu, *J. Am. Chem. Soc.*, 2011, **133**, 15810–15813.

